



DNAzyme Cleavage of CAG Repeat RNA in Polyglutamine Diseases

Nan Zhang¹ · Brittani Bewick¹ · Jason Schultz¹ · Anjana Tiwari¹ · Robert Krencik² · Aijun Zhang³ · Kaho Adachi⁴ · Guangbin Xia⁵ · Kyuson Yun¹ · Partha Sarkar⁶ · Tetsuo Ashizawa¹

Accepted: 11 June 2021 / Published online: 23 June 2021
© The Author(s) 2021

Abstract

CAG repeat expansion is the genetic cause of nine incurable polyglutamine (polyQ) diseases with neurodegenerative features. Silencing repeat RNA holds great therapeutic value. Here, we developed a repeat-based RNA-cleaving DNAzyme that catalyzes the destruction of expanded CAG repeat RNA of six polyQ diseases with high potency. DNAzyme preferentially cleaved the expanded allele in spinocerebellar ataxia type 1 (SCA1) cells. While cleavage was non-allele-specific for spinocerebellar ataxia type 3 (SCA3) cells, treatment of DNAzyme leads to improved cell viability without affecting mitochondrial metabolism or p62-dependent aggresome formation. DNAzyme appears to be stable in mouse brain for at least 1 month, and an intermediate dosage of DNAzyme in a SCA3 mouse model leads to a significant reduction of high molecular weight ATXN3 proteins. Our data suggest that DNAzyme is an effective RNA silencing molecule for potential treatment of multiple polyQ diseases.

Keywords DNAzyme · Polyglutamine · CAG repeats · Huntington's disease · Spinocerebellar ataxia · Microsatellite expansion

Introduction

DNAzymes (Dzs) are single-stranded RNA-cleaving DNAs that typically consist of a catalytic core and two flanking RNA-binding arms for target recognition. The catalytic core

cleaves a phosphodiester bond in the presence of divalent cations, generating a 5'-product with a 2',3'-cyclic phosphate at the 3'-end and a 3'-product with a hydroxyl group at the 5'-end. The 8–17 DNAzyme is among the first identified DNAzymes that efficiently cleave RNA substrates [1]. The

✉ Nan Zhang
nzhang@houstonmethodist.org

Brittani Bewick
bbewick@houstonmethodist.org

Jason Schultz
jschultz@houstonmethodist.org

Anjana Tiwari
atiwari@houstonmethodist.org

Robert Krencik
rkrencik@houstonmethodist.org

Aijun Zhang
AZHANG@houstonmethodist.org

Kaho Adachi
adachikaho@berkeley.edu

Guangbin Xia
guangbin.xia@gmail.com

Kyuson Yun
kyun@houstonmethodist.org

Partha Sarkar
pssarkar@utmb.edu

Tetsuo Ashizawa
tashizawa@houstonmethodist.org

¹ Department of Neurology, Neuroscience Program, Houston Methodist Research Institute, Houston, TX, USA

² Center for Neuroregeneration, Department of Neurosurgery, Houston Methodist Research Institute, Houston, TX, USA

³ Center for Bioenergetics, Department of Neurosurgery, Houston Methodist Research Institute, Houston, TX, USA

⁴ Department of Molecular and Cell Biology, UC-Berkeley, Berkeley, CA, USA

⁵ Indiana University School of Medicine-Fort Wayne, Fort Wayne, IN, USA

⁶ Department of Neurology and Department of Neuroscience, Cell Biology and Anatomy, UTMB Health, Galveston, TX, USA

15-nucleotide (nt) core has been independently isolated under different cation selections such as Mg^{2+} , Mn^{2+} , Ca^{2+} , Zn^{2+} , and Pb^{2+} and shown to twist into a pseudoknot with the two RNA binding arms 70° apart in the crystal structure [2]. Despite their high reprogrammability and versatility for chemical modification and nanoconjugation, the therapeutic value and means of delivery are largely unexplored.

Polyglutamine (polyQ) diseases are a group of incurable neurodegenerative disorders caused by CAG repeat expansion in coding regions, including Huntington's disease (HD), spinocerebellar ataxias (SCA types 1, 2, 3, 6, 7, and 17), dentatorubropallidoluysian atrophy (DRPLA), and spinobulbar muscular atrophy (SBMA) [3]. A toxic gain of function of the expanded polyQ proteins has been proposed to cause a variety of potential pathogenic cellular events, including single- or double-stranded (ss/ds) DNA breaks [4–9], impaired protein homeostasis [10–13], transcription dysregulation [14, 15], protein sequestration [16, 17], disruption of nucleocytoplasm transport and endoplasmic reticulum architecture [16, 18–20], and mitochondrial dysfunction [21–23] in different diseases. In addition, the expanded RNA can also give rise to noncanonical repeat-associated non-ATG (RAN) translation products [24–26]. Thus, ridding cells of the mutant polyQ RNA/protein has become a major disease intervention and its success is thought to ameliorate any downstream pathomechanistic defects.

Significant progresses have been made through CRISPR-Cas genome editing and antisense oligonucleotide (ASO) therapies in many polyQ diseases, especially in HD, SCA2, and SCA3 [27–38]. Efforts towards engineering high-fidelity Cas proteins with various controller modules, split Cas proteins for efficient viral packaging, and non-viral delivery approaches are underway to improve precision and safety [39–42]. ASOs have been successfully tested in HD, SCA1, SCA2, SCA3, and SCA7 cells or mouse models and with HD ASO entering the Phase III clinical trial [30, 33, 34, 36, 37, 43–45]. The efficacy of ASO may vary from case to case and may largely depend on RNase H activity, accessibility of target sites, design chemistry, and bioavailability in target tissue. Observations from clinical trials and animal studies suggest that targeting both mutant and normal alleles of the polyQ protein does not associate with any pathology or deleterious side effects. In addition, no off-target effects were detected using CAG complementary ASOs in HD and SCA3 patient cells or HD Q175 mice [46–48]. The above observations have clearly outlined the possibility and benefit of using a single repeat-based agent to reduce mutant polyQ RNA and protein load across multiple diseases.

Since the 8–17 core cleaves the phosphodiester bond between ribonucleotides A and G, we designed an 8–17 DNAzyme that binds to and cleaves CAG repeat RNA. We demonstrate that the designer DNAzyme cleaves its target in the presence of different ions and under physiological concentrations. The chemically stabilized DNAzyme retains

the catalytic activity and knocks down or eliminates mutant polyQ RNA or protein load in cells from several polyQ disease origins and high molecular weight (HMW) ATXN3 proteins in a SCA3 mouse model.

Materials and Methods

General Methods and DNA

Unmodified DNA oligonucleotides were purchased from Sigma-Aldrich. PNA oligonucleotides were purchased from PNA Bio. LNA oligonucleotides were purchased from Qiagen. Q5 high-fidelity DNA polymerase (New England Biolabs) was used for routine PCR amplification. Restriction digestion and ligation were performed with FastDigest enzymes and T4 DNA Ligase Kit (Thermo Fisher Scientific), respectively. DNA plasmids were propagated in chemically competent *Escherichia coli* Stbl3 (Thermo Fisher Scientific) and sequenced at GENEWIZ.

HEK293 and SH-SY5Y cells were cultured at 37°C with 5% CO_2 in Dulbecco's modified Eagle's medium (DMEM, GIBCO) containing 10% non-inactivated fetal calf serum (FBS, GIBCO) and 100 U/ml penicillin–streptomycin (P/S, GIBCO). Normal (GM23973) and patient-derived SCA1 (GM06927, 52/29 CAG repeats) and SCA3 (GM06151, 74/24 CAG repeats) fibroblast cells were purchased from Coriell Cell Repositories and cultured in DMEM supplemented with 10% FBS and 1% P/S. Fibroblasts used in this study are no more than 2 passages different across cell lines and are all below 15 passages for nucleofection. BMECs (brain microvascular endothelial cells, gift of Dr. Kyuson Yun) were cultured on plates coated with $2\ \mu\text{g}/\text{cm}^2$ fibronectin at 37°C in Medium 199 (Gibco) containing 5% NuSerum, 5% FBS, and 1% P/S. Normal WTC11 iPSCs (GM25256) were purchased from Coriell Cell Repositories. Different iPSC lines were cultured in TeSR™-E8™ (STEMCELL Technologies) on plates or round coverslips coated with Matrigel (Corning).

The expanded *ATXN1* (gift of Dr. Huda Zoghbi), *TBP* (gift of Dr. Shihua Li), *ATXN7* (gift of Dr. Harry Orr), and *AR* (Addgene #28,235) genes were cloned from their parental backbones into pCMV-(DYKDDDDK)-N vector to acquire a FLAG tag (Clontech). The pEGFP-Q74 (for HTTex1, #40,262), pEGFP-C1-ATXN3-Q28 (#22,122), and pEGFP-C1-ATXN3-Q84 (#22,123) plasmids were purchased from Addgene.

Animals

All animal procedures were approved by the Houston Methodist Institutional Animal Care and Use Committee and conducted in compliance with the National Institutes

of Health guidelines for the use of experimental animals. Genotyping was performed using tail biopsy DNA isolated prior to weaning. PCR was performed using Qiagen DNeasy Blood and Tissue Kit and primers recommended by the Jackson Laboratory to amplify a fragment of the *ATXN3* transgene. Animals were matched for age, sex, and weight for this study. Six-month old animals were injected with either saline or DNAzyme and brain tissues were harvested after 1 month for imaging and biochemical analyses. Before euthanization, blood was drawn and analyzed for clinical chemistry and hematology at the MD Anderson core facility. Different experimental stages—such as injection, brain harvest, and biochemical assays—were carried out by different personnel to ensure data reproducibility.

In vivo Imaging System (I.V.I.S.) and Stereotaxic Injection

I.V.I.S. imaging was performed using a Caliper Xenogen 200 system, and images were normalized using the Living Image Software.

“Naked” DNAzyme resuspended in PBS was stereotaxically administered into the right lateral ventricle. Intracerebroventricular (i.c.v.) injections were performed on mice under intraperitoneal ketamine anesthesia. For each i.c.v. injection, a small incision was made to expose the Bregma and a small hole was drilled at the coordinates pre-determined by the NeuroStar software (mediolateral + 1 mm; anterior–posterior – 0.3 mm; dorsoventral – 2.5 mm). Four hundred μg LNA8-17Dz9 was delivered at an infusion rate of 4 turns/min using a Hamilton syringe on a Global Biotech stereotaxic instrument. After the injection was complete, the needle was slowly retracted at a rate of 1 mm/min and animals were sutured and supplied with a painkiller.

RNA In vitro Transcription and Cleavage Assay

CAG_{x30} and CAG_{x42} were cloned into pcDNA3.1-hygro+ at NheI and HindIII sites, linearized at the EcoRV site, and in vitro transcribed at 30 °C overnight using HiScribe T7 High Yield RNA Synthesis Kit (NEB) with approximately 500 ng of DNA input. The transcribed RNA was digested with TURBO DNase I at 37 °C for 30 min before column purified using RNA Clean and Concentrator (Zymo Research).

RNA cleavage assays were performed in 1 × Dz digestion buffer (50 mM Tris–HCl pH 7.5, 150 mM NaCl and varying concentrations of Mg²⁺ or Ca²⁺) with 100 nM target RNA and 500 nM 8-17Dz at 37 °C for the indicated time. Samples were quenched in 2 × TBE-Urea Loading Buffer (Bio-Rad) mixed with 3 × formamide dye (100% formamide, 0.5 M EDTA), boiled at 95 °C for 5 min, and loaded on 10% TBE-Urea gels. After running at 200 V for approximately

1 h, RNA cleavage was detected in SYBR Gold (Invitrogen, 1:50,000) on an Azure c400 Biosystem.

Transfection

HEK293 or SH-SY5Y cells were seeded at 700,000 per well (6-well format), approximately 16 h before transfection. Transfection was performed with 2 μg plasmid DNA \pm 200 pmol 8-17Dz in the presence of 15 μl Lipofectamine 2000 (Invitrogen) according to the manufacturer’s instruction.

Fibroblasts were nucleofected using the P2 Primary Cell 4D-Nucleofector X Kit (100 μl format) on a 4D-Nucleofector X unit (Lonza) according to the manufacturer’s instruction. One million cells combined \pm 200 or 300 pmol DNAzyme were nucleofected under the program “CZ167” and plated in pre-warmed medium in each well. Analyses (immunoblot/IF/functional assays) were performed 48 h post transfection.

Each 100-pmol DNAzyme was transfected with 1.5 μl Lipofectamine Stem Reagent (Thermo Fisher Scientific) into iPSCs or differentiating iNeurons according to the manufacturer’s protocol.

RNA Isolation and Quantitative RT-PCR (qRT-PCR)

Total RNA was isolated using RNeasy Mini Kit (Qiagen), digested with TURBO DNase I (Thermo Fisher Scientific), and purified using RNA Clean and Concentrator (Zymo Research) according to the manufacturer’s protocol. One microgram of input RNA was reverse transcribed using iScript cDNA Synthesis Kit (Bio-Rad). PCR amplification was performed with 2.5 μl of diluted cDNA (1:3 dilution) on a CFX96 Real-time System (Bio-Rad). RNA expression was normalized against that of *GAPDH*, and the relative normalized expression was calculated using CFX Manager 3.1 (Bio-Rad).

DCL64 Liposome Packaging

1,2-Dipalmitoyl-sn-glycero-3-phosphocoline (DPPC) and cholesterol were purchased from Avanti Polar Lipids and poloxamer L64 was purchased from Sigma-Aldrich. DCL64 liposomes were prepared by mixing DPPC, cholesterol, and poly(ethylene glycole)-block-poly(propylene glycol)-block-poly(ethylene glycol) L64 (poloxamer L64) at a 5:3:7 weight ratio at room temperature. DNAzyme was mixed with DCL64 at a 1:10 weight ratio at room temperature. All DCL64 liposomes were prepared in Wheaton glass vials and mixed with excess tert-butanol at room temperature prior to freezing at – 80 °C overnight. The DCL64 liposomes were then lyophilized overnight, using a FreeZone 2.5 lyophilizer (Labconco), until a thin film had formed, and there was no evidence of liquid within the glass vial. DCL64 liposomes

not needed for use immediately were stored at -20°C . The DCL64 liposomes were reconstituted with sterile $1\times\text{PBS}$ to the desired concentration immediately before use.

DNA Tetrahedron Assembly and Packaging

PAGE-purified DNA oligonucleotides (Table S3) were purchased from Sigma-Aldrich. DNA tetrahedra were generated by mixing equimolar quantities ($1\ \mu\text{M}$) of each strand ($\pm\text{DNAzyme}$) in $1\times\text{TM}$ buffer ($20\ \text{mM}$ Tris-HCl pH 7.5, $50\ \text{mM}$ $\text{MgCl}_2\cdot\text{H}_2\text{O}$), and the mixture was slowly cooled from 95 to 25°C over 2 h. The assembled structure was characterized by 1% agarose gel and 4% native PAGE gel. Two assembly reactions were pooled (equivalent to $200\ \text{pmol}$ of DNAzyme) for cell delivery.

Protein Isolation and Immunoblot

Proteins were isolated from cells 48 h post transfection and lysed in Pierce IP Lysis Buffer (Thermo Fisher Scientific) supplemented with cOmplete Protease Inhibitor Cocktail (Roche) and PhosSTOP (Sigma-Aldrich) at 4°C for 30 min. Soluble fractions were collected after centrifugation at $13,200\ \text{rpm}$ at 4°C for 15 min and quantified using Pierce BCA Protein Assay Kit (Thermo Fisher Scientific).

For immunoblot analysis, approximately $40\ \mu\text{g}$ of proteins were denatured in $4\times\text{Laemmli}$ Sample Buffer (Bio-Rad) and β -mercaptoethanol at 95°C for 5 min before loaded on 4–15% SDS-PAGE gels (Bio-Rad). Proteins were transferred onto PVDF membranes (Bio-Rad) using a Mini Trans-Blot Electrophoretic Transfer Cell (Bio-Rad) at 100 V for approximately 1.5–2 h at 4°C . Membranes were incubated with blocking buffer (5% Blotting-Grade Blocker, Bio-Rad, in $1\times\text{TBST}$, 0.1% Tween 20) at room temperature for 1 h, followed by primary antibody incubation at 4°C overnight and secondary antibody incubation at room temperature for 1 h. Chemiluminescent signals were detected using SuperSignal West Pico Chemiluminescent Substrate (Thermo Fisher Scientific) on an Azure c400 Biosystem and quantified using ImageJ.

Right cortical tissues from mouse brain were flash frozen for protein analysis. Total protein lysate was extracted using mechanical homogenization in $500\ \mu\text{l}$ RIPA buffer containing cOmplete mini protease inhibitor cocktail and PhoStop phosphatase inhibitor. Homogenate was incubated at 4°C with agitation for 2 h prior to clearing the debris via centrifugation at $12,000\ \text{rpm}$ for 20 min at 4°C . Supernatants were used for immunoblotting analysis.

Primary antibodies used in this study include mouse anti-ATXN1 (2F5, 1:1,000, Thermo Fisher Scientific), rabbit anti-ATXN2 (NBP1-90,063, 1:200, Novusbio), mouse anti-ATXN3 (MAB5360, 1:1,000, Millipore), rabbit anti-ATXN3 (13,505-1-AP, 1:500, Proteintech),

mouse anti-FLAG (M2, 1:1,000, Sigma-Aldrich), mouse HRP-conjugated GAPDH (HRP-60004, Proteintech), mouse anti-GFP (GF28R, 1:1,000, Thermo Fisher Scientific), mouse anti-polyglutamine (MAB1574/5TF1-1C2, 1:1,000, Millipore), rabbit anti-Oct4 (#2750, 1:200, Cell Signaling Technology), rabbit anti-Sox2 (D6D9, 1:200, Cell Signaling Technology), rabbit anti-Nanog (D73G4, 1:200, Cell Signal Technology), mouse anti-8-OHdG (E-8, 1:200, Santa Cruz Biotechnology), rabbit anti-ATXN7 (PA1-749, 1:1,000, Thermo Fisher Scientific), mouse anti-TBP (1TBP18, 1:1,000, Thermo Fisher Scientific), and mouse anti-p62/SQSTM1 (D-3, 1:500, Santa Cruz Biotechnology).

iNeuron Differentiation and Harvest

iNeurons were differentiated as previously described [49]. Briefly, WTC11 iPSCs with integrated hNGN2 were cultured on 6-well plates coated with Matrigel and induced in cortical neuron culture medium (DMEM/F12 with HEPES, $1\times\text{B27}$ supplement, doxycycline $2\ \mu\text{g}/\text{ml}$). On day 3, cells were individualized by Accutase (STEMCELL Technologies), seeded on Matrigel coated 6-well plates, and transfected using Lipofectamine Stem Transfection Reagent with HTTex1-Q74 $\pm\text{DNAzyme}$ (total DNA: LipoStem ratio is 1:2) according to the manufacturer's protocol. Cells were harvested for immunoblot or imaging on day 5 and day 7.

Generation of SCA3 iPSC

The study was approved by the University of Florida Institutional Review Board. The SCA3 subject was provided with the approved informed consent. Skin biopsy was performed by punch biopsy (6 mm in diameter) under local anesthesia. The skin specimens were placed in sterile DMEM medium supplemented with 20% FBS and 1% P/S at room temperature for transport to the lab. Biopsy specimens were processed into 0.5-mm cubes and placed into duplicate $25\ \text{cm}^2$ flasks. The explants were air-dried for 30 min and 12 ml of primary culture medium (DMEM with 20% FBS) was added to the flask. The flasks were placed in a 37°C 5% CO_2 incubator. The medium was replenished after 7 days. When fibroblasts from adjacent explants started to merge, the flasks were treated with 0.05% Trypsin/EDTA and passed to a $75\ \text{cm}^2$ flask. These cells were designated as passage 1. Passage 3 fibroblasts were used for reprogramming.

Reprogramming was performed by a non-integrating method using CytoTune Sendai Reprogramming Kit (Thermo Fisher Scientific) on the fibroblasts according to the manufacturer's protocol as previously published [50]. Isolated iPSC clones were cultured on either vitronectin- or Matrigel-coated plates in TeSR-E8 medium (STEMCELL Technologies).

Fluorescent Microscopy and Immunofluorescence (IF)

To evaluate DNAzyme's cellular uptake, BMEC or SH-SY5Y cells were incubated with naked or DCL64-packaged Cy3-LNA8-17Dz9 for 48 h, washed five times with PBS (5 min each), fixed in 4% paraformaldehyde (PFA) solution in PBS (Thermo Fisher Scientific) for 10 min, permeabilized in 0.2% Triton X-100 in PBS for 10 min, and mounted in Mounting Medium with DAPI for Fluorescence (Vectorshield). Images were taken on a Nikon A1 Confocal Imaging system.

IF was carried out 48 h post transfection. Fibroblasts, iPSCs, or iNeurons on coverslips were washed with PBS, fixed in 4% PFA, permeabilized in 0.2% Triton X-100 in PBS, and blocked in 5% BSA in PBST (0.05% Tween 20). Primary antibody incubation was carried out at 4 °C overnight, followed by fluorophore-tagged secondary antibody incubation at room temperature for 1 h before mounting in DAPI medium. A Nikon A1 Confocal Imaging system was used.

After brain harvest, sagittal sections of all mouse brains were fixed in 4% PFA for 48 h, cryoprotected in a sucrose gradient, and embedded in OCT. Cryostat sections from OCT embedded tissue were cut at 10 μm thickness and mounted on slides. Sections were fixed in 4% PFA, washed in PBS, and blocked in 5% normal goat serum, 0.2% Triton X-100 in PBS. Sections were then incubated in mouse anti-GFAP antibody (1:500, sc-33673, Santa Cruz Biotechnology) at 4 °C overnight. After washing, the sections were incubated in secondary antibody, washed in PBS, and mounted in Mounting Medium with DAPI (Vectorshield). Slides were imaged with a Nikon A1 Confocal Imaging system.

Cell Proliferation Assay

Cell proliferation was assessed using the Aqueous One Solution Cell Proliferation Assay (Promega). In brief, 5000 cells (\pm nucleofected DNAzyme) were plated in each 96 well and treated with 20 μl MTS at 37 °C for 3 h. Absorbance at 490 nm was recorded on a PerkinElmer EnSpire Multimode Plate Reader.

Mitochondrial Membrane Potential Assay

Mitochondrial membrane potential was measured using the JC-10 dye according to the manufacturer's protocol (G-Biosciences). In brief, 5000 cells (from the same nucleofection used for cell proliferation assays) were plated in each of the 96 wells, incubated with 100 μl JC-10 solution (1: 200 dilution) for 20 min at 37 °C, washed twice with 1 × MMP solution (1: 5 dilution), and recorded at excitation/

emission 535 nm/595 nm and 485 nm/535 nm on the EnSpire plate reader. The red-to-green fluorescence ratio was used for plotting the graph.

RNAseq

Normal fibroblasts were nucleofected without or with 200 pmol LNA8-17Dz9 (mock vs Dz200) as described above (2 biological replicates for each). After 48 h, total RNA was isolated using RNeasy Mini Kit (Qiagen), treated with DNase I, and purified using RNA Clean and Concentrator (Zymo Research). The quality of RNA was assessed using Agilent 2100 at Novogene; all samples have a RIN number > 8. The library was constructed at Novogene and RNA-seq was carried out with Illumina NovaSeq 6000 PE150 at 20 M depth. Raw reads were processed with fastp (version 0.20.1), mapped to the human reference genome (GRCh38 and Ensembl gene annotation) with STAR (version 2.7.6a), sorted with SAMtools (version 1.9), and finally counted with HTSeq-count (version 0.11.2) under the miniconda environment. Raw counts were normalized to counts per million mapped reads (CPM), and subsequently FDR, p-value and LogFC were calculated with Degust. Genes were considered significantly differentially expressed at FDR < 0.25 and p-value < 0.05, or |Log2FC| > 1.5 and FDR < 0.05.

Statistical Analysis and Image Processing

Statistical analyses of all data were performed using *t*-test in GraphPad Prism Version 7.03 (**P* < 0.05, ***P* < 0.01, ****P* < 0.001, *****P* < 0.0001).

Quantification of p62 aggresome/cell was performed in Fiji ImageJ. p62 foci were counted using "Find maxima" with the threshold set to 60. Cells were counted in 8-bit images with threshold set to 30–255 and particle size set to 60–infinity.

Results

Designer DNAzyme 8–17 (8-17Dz) Cleaves CAG Repeat RNA Biochemically

As a proof-of-concept experiment, three 8-17Dzs with varying lengths of CAG complementing arms were initially designed and tested for cleavage efficiency of in vitro transcribed CAG_{x30} RNA (Fig. 1A). Although the highest activity of the 8-17Dz core is normally observed in the presence of Pb²⁺ [51], we decided to initially screen with Mg²⁺—one of the most abundant metal ions in biological fluids. Among the three 8-17Dz designs, the 8-17Dz with 9-nt-binding arms (8-17Dz9) exhibits the highest RNA cleavage activity across the tested range of Mg²⁺

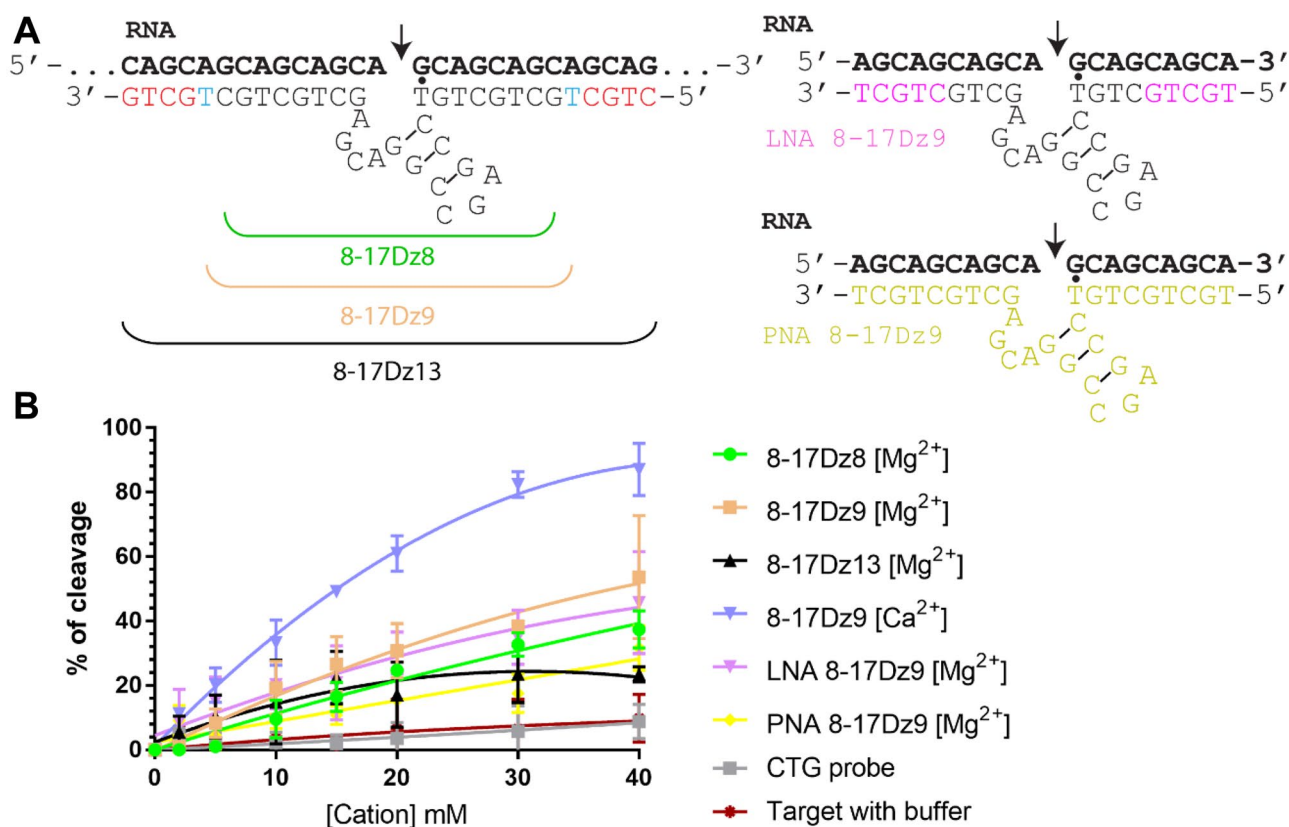


Fig. 1 DNAzyme design and biochemical activity. **A** Designs of 8-17Dzs with different RNA binding arms' lengths. Locked nucleic acids (LNAs) are highlighted in magenta, and peptide nucleic acids (PNAs) are highlighted in yellow. The T·G mismatch is indicated. **B**

Biochemical RNA cleavage assays at 37 °C for 1 h under different cation concentrations ($n=3$). A CTG probe complementary to the CAG RNA repeats were used as a negative control

concentrations over 1 h (Figs. 1B and S1). Additional alterations of RNA-binding arm's length changed the catalytic property of 8-17Dz to different extents (Fig. S2). Further analysis using Ca^{2+} as a cofactor shows superior RNA cleavage efficiency compared to Mg^{2+} (Figs. 1B and S1). To test if the 8-17Dz9 could work under low Mg^{2+} concentrations, RNA cleavage was assayed in the presence of 5 mM Mg^{2+} (Fig. S3). Direct and indirect measurement of total cellular Mg^{2+} concentration by various techniques consistently indicates that total Mg^{2+} ranges between 17 and 20 mM in mammalian cells [52–54]. Although the cytosolic Mg^{2+} concentration in the occipital lobes of the human brain was estimated close to 200 μM [55], the Mg^{2+} concentration in the rest of the brain is largely uninvestigated. In addition, the majority of Mg^{2+} ions are complexed to a broad spectrum of biomolecules, such as nucleotides, and Mg^{2+} is an important counterion for stabilizing DNA (1 to 2 M counterions for distances between the DNA helix axes of 2–4 nm [56]). It is possible that DNAzyme functions as a Mg^{2+} sink and carries out catalysis under physiologically relevant influx/efflux of Mg^{2+} . The intracellular Ca^{2+} ions (approximately 100 nM [57]) and other divalent cations

may further contribute to DNAzyme's activity. As shown in Fig. S3, approximately 50% of the target CAG_{x30} RNA were cleaved by 8-17Dz9 in 5 h at 5 mM Mg^{2+} . In agreement with our observation, the same 8–17 catalytic core has been successfully used to detect physiological $\text{Ca}^{2+}/\text{Mg}^{2+}$ levels in undiluted human blood serum [58]. Taken together, we demonstrate that the repeat-based 8-17Dz9 efficiently cleaves CAG RNA biochemically under low ionic strength and is activated by both Ca^{2+} and Mg^{2+} ions, potentially generating a compounding effect on CAG RNA cleavage in cells.

Locked Nucleic Acid Modification Retains 8-17Dz's Catalytic Activity

Unmodified DNAzyme is likely degraded by cellular nucleases; increased stability and affinity towards its target RNA may offer persistent therapeutic benefit in cells. Among the repertoire of chemical modifications, we chose the locked nucleic acid (LNA) and peptide nucleic acid (PNA) for base substitutions in 8-17Dz9 due to their strong binding affinity and incompatibility with RNase H [59–62]. We substituted the terminal five nucleotides of each binding

arm to LNA to create the LNA8-17Dz9 and all nucleic acids to PNA to create the PNA8-17Dz9 (Fig. 1A). To test if these modifications could affect DNAzyme function, we performed RNA cleavage assays at both high and low Mg^{2+} concentrations. The LNA8-17Dz9 retains comparable catalytic activity to that of the unmodified 8-17Dz9 (Figs. 1B and S3). PNA8-17Dz9 showed reduced RNA cleavage compared to the unmodified 8-17Dz9 (Figs. 1B and S3), possibly due to unfavorable folding of the peptidyl catalytic core, as global folding efficiency of DNAzyme has been linked to catalytic activity [63]. We further compared the DNAzyme's cleavage efficiency on two different in vitro transcribed CAG repeat lengths, CAGx30 and CAGx42 (Fig. S4). The LNA8-17Dz9 biochemically cleaves both RNA repeats with similar catalytic profiles.

LNA8-17Dz9 Significantly Knocks Down or Eliminates Multiple Mutant polyQ Proteins in HEK293 Cells

Huntington's disease is the most common inherited neurodegenerative disease and is caused by CAG repeat expansion in the first exon of Huntingtin (HTTex1 [64]). The mutant HTT (mutHTT) undergoes extensive autolysis and produces exon 1 fragments that aggregate in neuronal nuclei of brain tissue [65]. To test if DNAzyme could knock down mutHTTex1, we co-transfected an HTTex1 fragment containing 74Qs (HTTex1-Q74) with the three 8-17Dz9 designs in HEK293 cells for 48 h. We observed the highest *HTTex1-Q74* RNA knockdown by LNA8-17Dz9, followed by unmodified 8-17Dz9 and PNA8-17Dz9 (Fig. S5). At a protein level, the LNA8-17Dz9 showed the highest knockdown, followed by PNA8-17Dz9 and unmodified 8-17Dz9 (Fig. 2A). We further demonstrate that the observed protein knockdown is not due to competition of DNAzyme with polyQ plasmids during co-transfection by using a control DNA fragment of similar length (Fig. S6). The observed large variability in PNA8-17Dz9 transfected cells could be due to inconsistent packaging between the neutral amide PNA backbone and the cationic transfection lipids. To compare RNA silencing efficiency of our catalytic DNAzyme and RNase H-based antisense oligonucleotide, we designed an ASO containing the same binding arms and LNA modifications without the 8–17 catalytic loop. By targeting eGFP-HTTex1-Q74 in HEK293 cells, we show that LNA8-17Dz9 is approximately 10% more efficient at clearing the expanded polyQ proteins than the ASO counterpart (Fig. S7). Given that LNA8-17Dz9 is most effective in reducing RNA and protein load of mutHTTex1, it was used for the subsequent experiments.

CAG expansion in ataxin 1 (ATXN1), TATA binding protein (TBP), ataxin 7 (ATXN7), and androgen receptor (AR) causes SCA1, SCA17, SCA7, and SBMA, respectively. Each

mutant polyQ protein was cloned to acquire a FLAG tag and subsequently co-transfected with LNA8-17Dz9 in HEK293 cells for immunoblot analysis. LNA8-17Dz9 completely eliminates TBP-Q94 and ATXN7-Q61 protein expression and significantly reduces ATXN1-Q83 and AR-Q40 protein levels by approximately 80% (Fig. 2B). Based on our calculated dosage of DNAzyme and cell density, we estimate that between 8 and 12 million DNAzyme molecules are available for intracellular targeting, if a 50% transfection is achieved. To evaluate allele specificity by LNA8-17Dz9, we co-transfected the DNAzyme with either ATXN3-Q28 or ATXN3-Q84 (mutant ATXN3 causes SCA3) in HEK293 cells. LNA8-17Dz9 completely eliminates both proteins (Fig. S8). In the subsequent competitive cleavage experiment, an equal weight of ATXN3-Q28 and ATXN3-Q84 plasmids was co-transfected with LNA8-17Dz9 for immunoblotting. When both proteins are present in HEK293 cells, we did not observe preferential targeting of ATXN3-Q84 over Q28 (Fig. S8). Taken together, the LNA8-17Dz9 efficiently clears a panel of mutant polyQ proteins in HEK293 cells.

LNA8-17Dz9 Significantly Reduces polyQ Protein Load in Neuroblastoma Cells and iNeurons

To test if LNA8-17Dz9 could work in neuron-like cells, HTTex1-Q74 and LNA8-17Dz9 were co-transfected into SH-SY5Y neuroblastoma cells. We observed a >90% target protein knockdown (Fig. 3A). Striatal and cortical neurons exhibit prominent cell loss in postmortem HD brain tissues [66]. To test efficacy in neurons, we utilized a wild-type (wt) human iPSC line stably expressing a doxycycline-inducible human neurogenin 2 (WTC11-hNGN2) at the safe-harbor *AAVS1* locus [67]. Upon induction, the WTC11-hNGN2 iPSCs rapidly differentiate into cortical excitatory neurons (iNeurons) [49, 67, 68]. On a 5-day differentiation scheme, the iNeurons produced dendrites and expressed neuronal markers NeuN and MAP2 (Fig. 3B). Co-transfection of HTTex1-Q74 and 200 pmol LNA8-17Dz9 on day 3 reduced the target protein load by 90% (Fig. 3C). On a 7-day differentiation scheme (transfection on day 3 and harvest on day 7), the iNeurons lost the transgene expression entirely due to the nature of transient transfection (Fig. S9). Taken together, the LNA8-17Dz9 reduces approximately 90% of the polyQ protein load in neuroblastoma cells and iPSC-derived cortical neurons.

LNA8-17Dz9 Targets Both Normal and Expanded ATXN3 Alleles Without Affecting p62-Aggresome Levels in SCA3 iPSCs

SCA3 is the most common inherited ataxia and is caused by a CAG repeat expansion in the *ATXN3* gene [69].

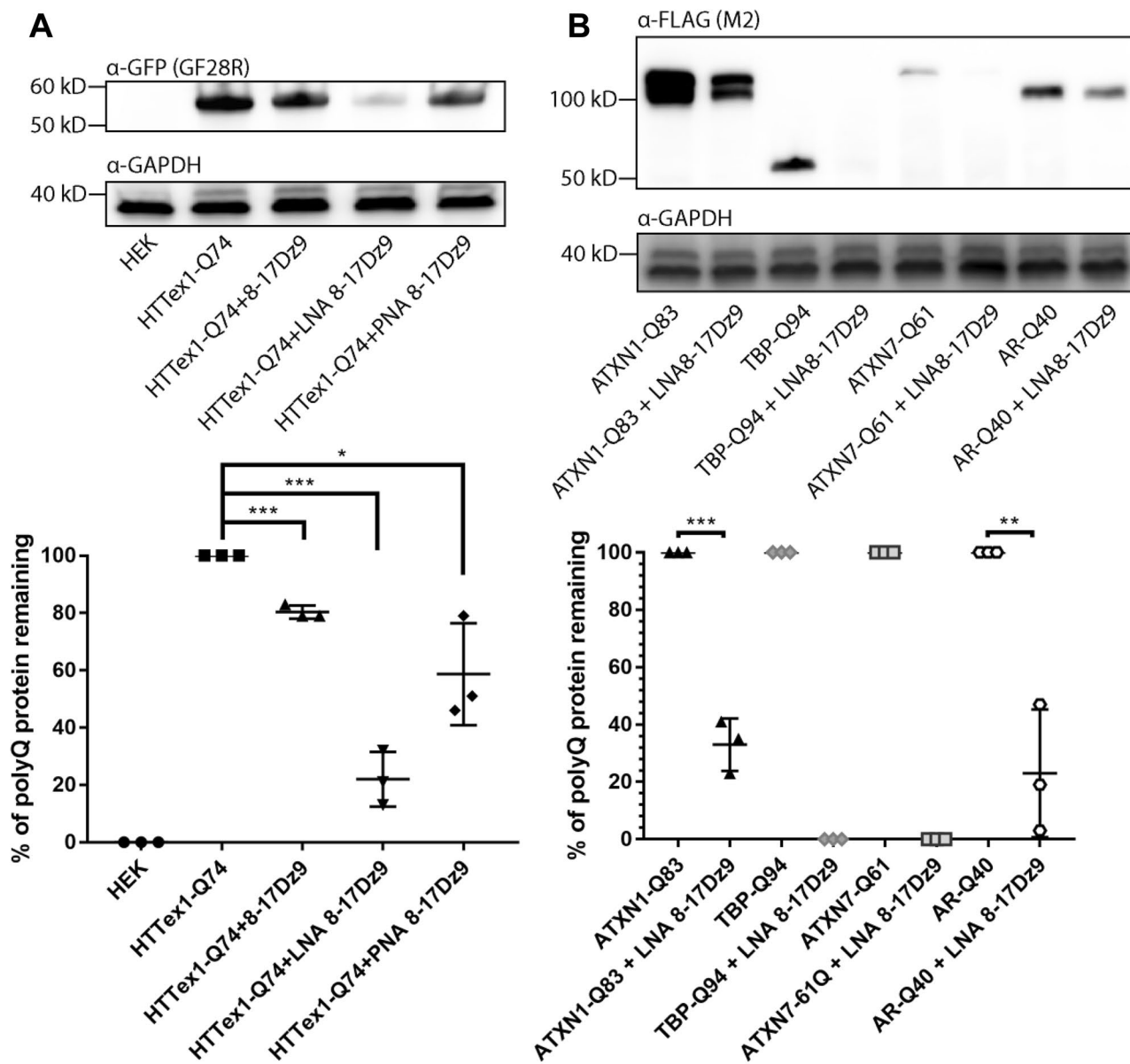


Fig. 2 DNAzyme effectively knocks down or eliminates an array of expanded polyQ proteins. **A** HTTex1-Q74 protein knockdown using three 8-17Dz designs (200 pmol each, or 80 nM) in HEK293 cells. **B**

Mutant ATXN1-Q83 (both bands were used for quantification), TBP-Q94, ATXN7-Q61, and AR-Q40 were significantly reduced or eliminated by 200 pmol (80 nM) LNA 8-17Dz9 in HEK293 cells

Although its role as a deubiquitinase has been associated with aggresome formation, autophagy, antiviral response, and transcription-coupled DNA repair [7, 69–74], different *Ataxin3*-knockout (KO) mice exhibit normal viability and fertility, suggesting that its function may not be essential [75, 76]. Thus, lowering the expression of both wild-type and mutant ATXN3 may be well tolerated. We have generated a patient-derived SCA3 iPSC line that expresses pluripotency markers Oct4, Sox2, and Nanog and has a repeat size close to CAG_{x80} (Figs. 3D and S10). Transfection of 200 pmol or 300 pmol of LNA8-17Dz9 showed similar

knockdown of both wtATXN3 and mutATXN3 proteins by approximately 40% (Fig. 3E); this non-allele-specific knockdown in iPSCs is consistent with observations in the overexpression system (Fig. S8). The autophagy-linked ubiquitin-binding shuttle protein p62 (SQSTM1) is known to co-localize with both wt and mutATXN3 proteins and promote perinuclear aggresome formation [33, 74, 77–79]. The non-allele-specific knockdown of ATXN3 in iPSCs did not show significant differences in p62-aggresome formation from untreated SCA3 iPSCs or normal WTC11 iPSCs (Fig. S11). Taken together, the LNA8-17Dz9 effectively

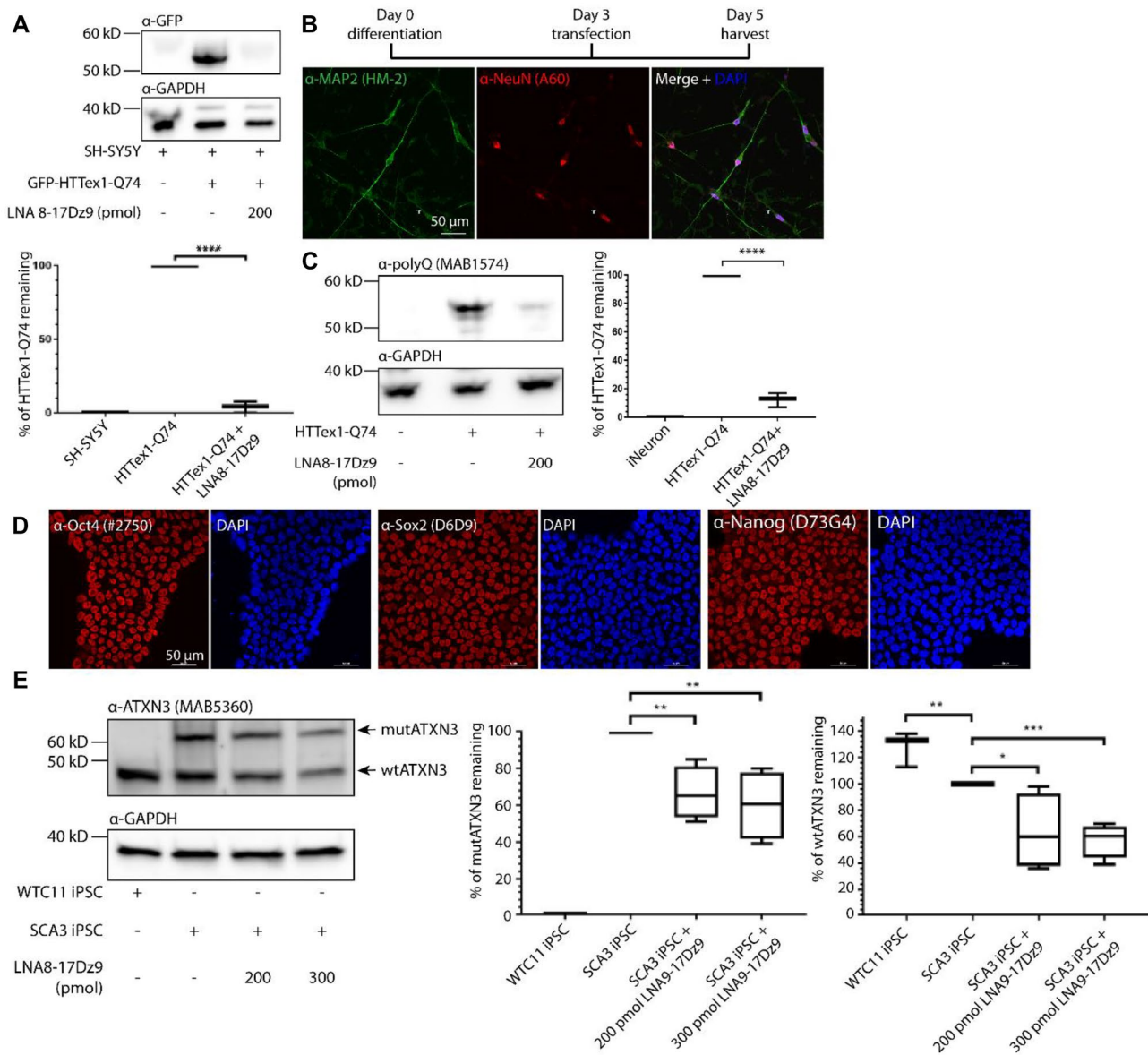


Fig. 3 DNAzyme significantly reduces polyQ protein targets in neuronal cells and iPSCs. **A** HTTex1-Q74 protein is significantly reduced in SH-SY5Y cells co-transfected with 200 pmol (80 nM) LNA8-17Dz9. **B** iNeuron differentiation scheme and immunofluorescence (IF) of 5-day differentiated iNeurons against neuronal markers NeuN and MAP2 (with antibody clone numbers indicated in brackets, $n=3$). **C** Immunoblot and quantification of transfected HTTex1-Q74

levels with or without 200 pmol (80 nM) LNA8-17Dz9 treatment in 5-day differentiated iNeurons ($n=3$). **D** IF of pluripotency markers in SCA3 iPSCs ($n=2$). **E** Immunoblot and quantification of mutant and wildtype ATXN3 in SCA3 iPSCs treated with 200 or 300 pmol (80 or 120 nM) LNA8-17Dz9 ($n=4$). The quantity of mutATXN3 in SCA3 iPSC (without treatment) was used as 100% for normalization

lowers both wild-type and mutant ATXN3 to a similar extent in SCA3 iPSCs without affecting aggresome formation and by inference p62-dependent autophagy.

Allele-Specific Targeting of Mutant polyQ Protein Can Be Achieved in Patient-Derived Fibroblasts

To further investigate if LNA8-17Dz9 could achieve allele specificity, SCA1 and SCA3 patient-derived fibroblasts were

nucleofected with either 200 or 300 pmol LNA8-17Dz9 for 48 h. In both cell lines, significant target knockdown *ATXN1* RNA in SCA1 and *ATXN3* RNA in SCA3 were observed (Fig. S12). In SCA1 fibroblasts, LNA8-17Dz9 preferentially reduces the mutATXN1 protein load (detected by the polyQ antibody as the ATXN1 antibody does not pick up mutATXN1) by 40–60% without affecting the wtATXN1 level (Fig. 4). It did not alter the wtATXN3 level but reduced the wtATXN2 level by approximately

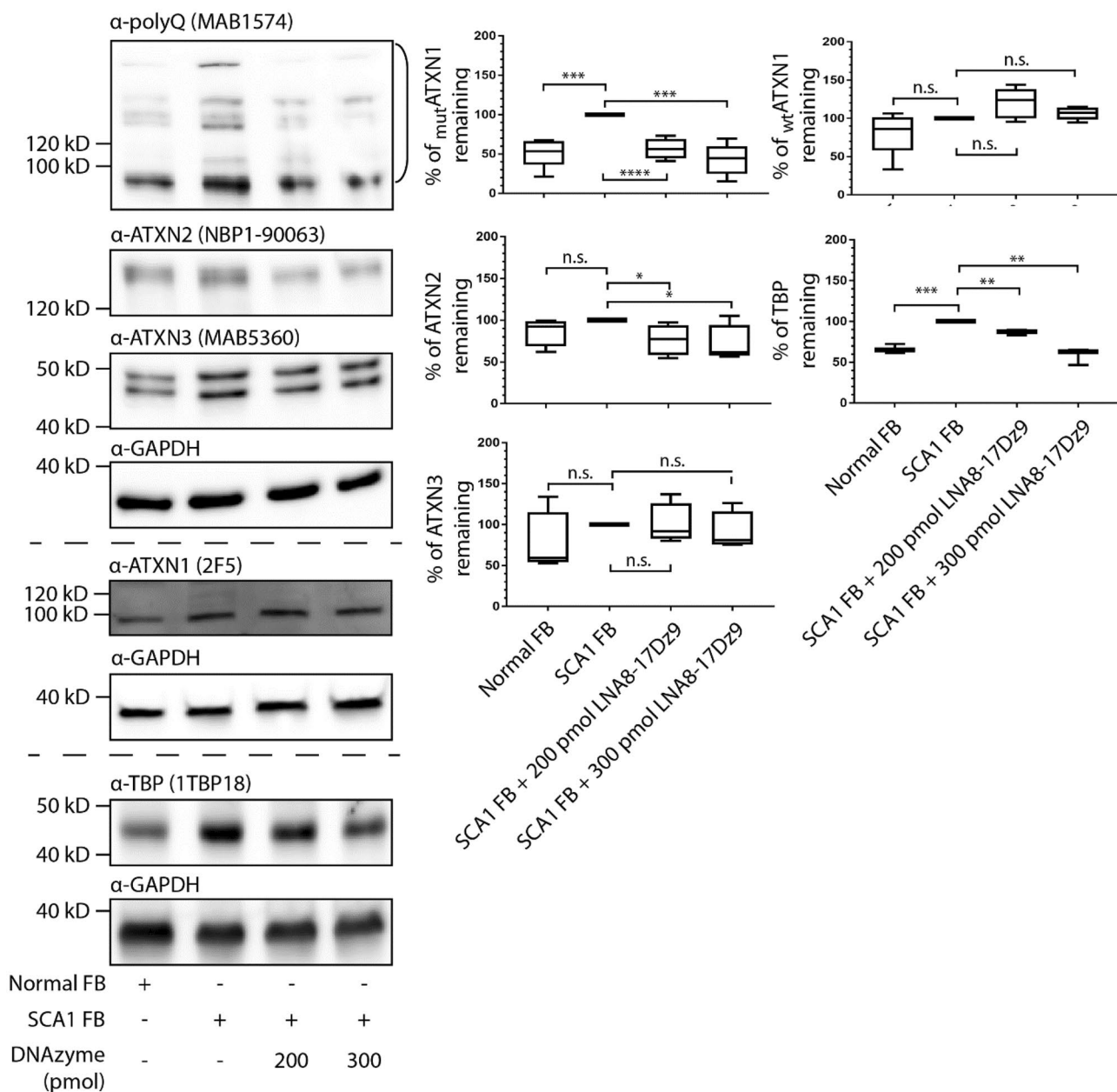


Fig. 4 Allele specificity can be achieved by DNAzyme in SCA1 fibroblasts. Immunoblot and quantification of SCA1 fibroblasts nucleofected with 200 or 300 pmol LNA8-17Dz9 (*n*=4). Protein bands

used for quantification of mutant polyQ proteins are highlighted by the open bracket. FB – fibroblast

30–40%. The LNA8-17Dz9 treatment reduced wtTBP to a level comparable to that in normal fibroblasts (Fig. 4). Even though ATXN3, ATXN2, and TBP all contain short CAG repeats, DNAzyme may affect their protein levels differentially (Fig. 4). Given that mutATXN1 may undergo aggregation, we assayed for insoluble fraction of protein post DNAzyme treatment and observed mutATXN1 knockdown by DNAzyme (Fig. S13). This observation is preliminary as there is not a good loading control in the insoluble fraction. In SCA3 fibroblasts, the LNA8-17Dz9 knocks down both

wtATXN3 and mutATXN3 by 40–50%, closely tracking the results obtained in SCA3 iPSCs (Fig. 5 vs. Fig. 3E). Consistent with SCA1 cells, the wtATXN1 level was not affected by DNAzyme treatment while the wtATXN2 level was reduced by approximately 40% and the wtTBP to a similar level as observed in normal fibroblasts (Fig. 5). The reason as to why DNAzyme suppressed wtATXN3 in SCA3 fibroblasts but not in SCA1 fibroblasts could be due to differences in wt allelic copies, as SCA3 fibroblasts have only one wtATXN3 allele while the tested SCA1 fibroblasts

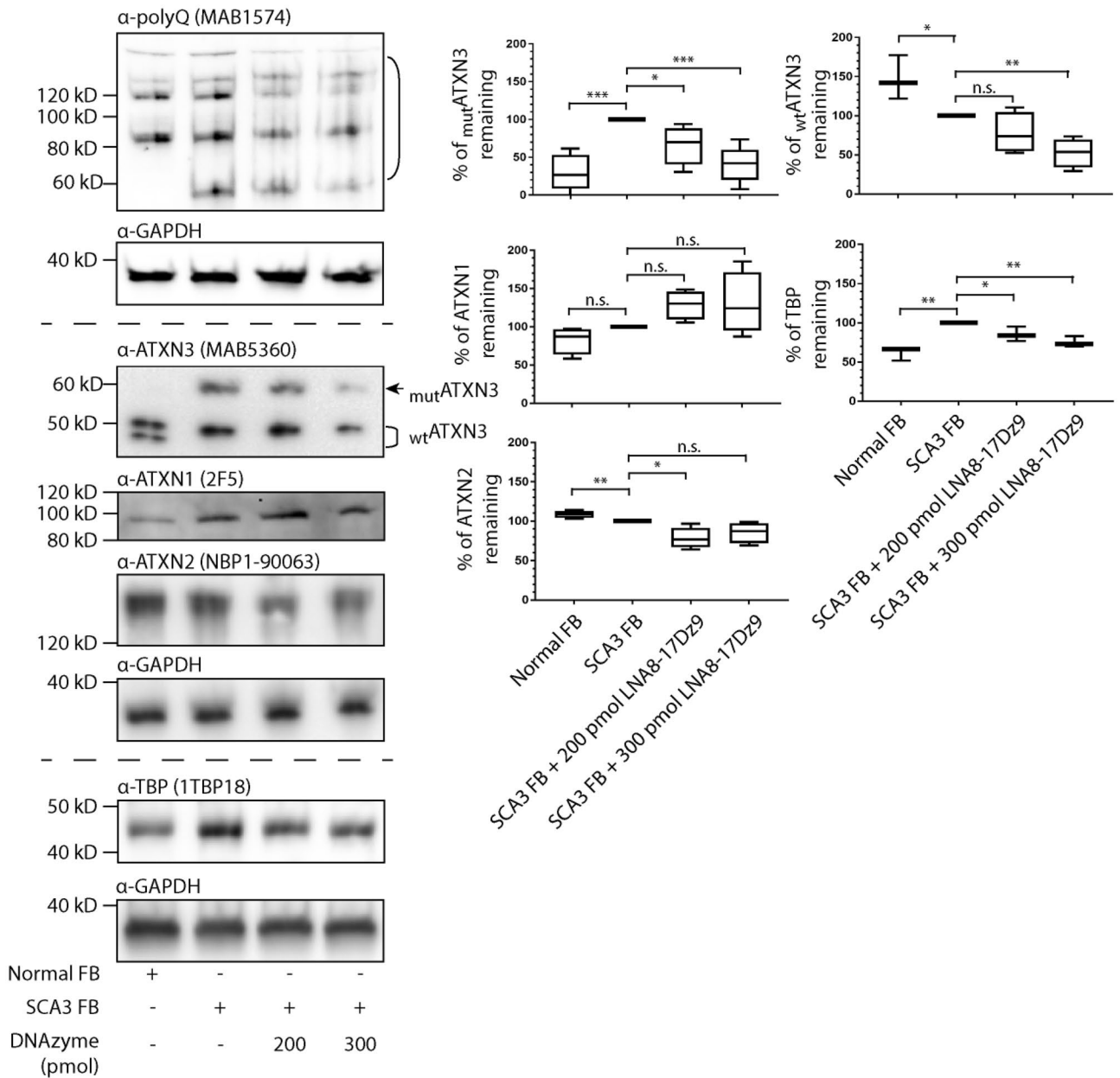


Fig. 5 DNazyme knocks down both wt and mutATXN3 in SCA3 fibroblasts. Immunoblot and quantification of SCA3 fibroblasts nucleofected with 200 or 300 pmol LNA8-17Dz9 (*n*=4). Protein bands

used for quantification of mutant polyQ proteins are highlighted by the open bracket. FB – fibroblast

have two. Such dosing effect could potentially be sensitive to DNazyme treatment. In addition, the observed knockdown of both allele and non-allele selective manners requires further mechanistic investigations on the targeting moiety. To investigate the potential off-target effects of using repeat-based DNazyme, we performed RNAseq analysis on mock- or LNA8-17Dz9-nucleofected wild-type fibroblast cells. By analyzing the expression of more than 60 published CAG-repeat containing mRNAs [80], we observed no significant transcriptomic off-target effects (Table S1).

The DNazyme-treated SCA3 fibroblasts were subject to further cell proliferation studies, given that potential off-target knockdown of wtATXN3, wtATXN2, and wtTBP was observed. To our surprise, the LNA8-17Dz9 treatment consistently improved SCA3 cell survival (even better survival than wt cells at low concentration, Fig. 6A). At a higher dosage of DNazyme (300 pmol), SCA3 cell survival improved by > 30% compared to that of mock-nucleofected SCA3 cells (Fig. 6A). The above data show that the on-target reduction of mutant polyQ protein clearly benefits SCA3

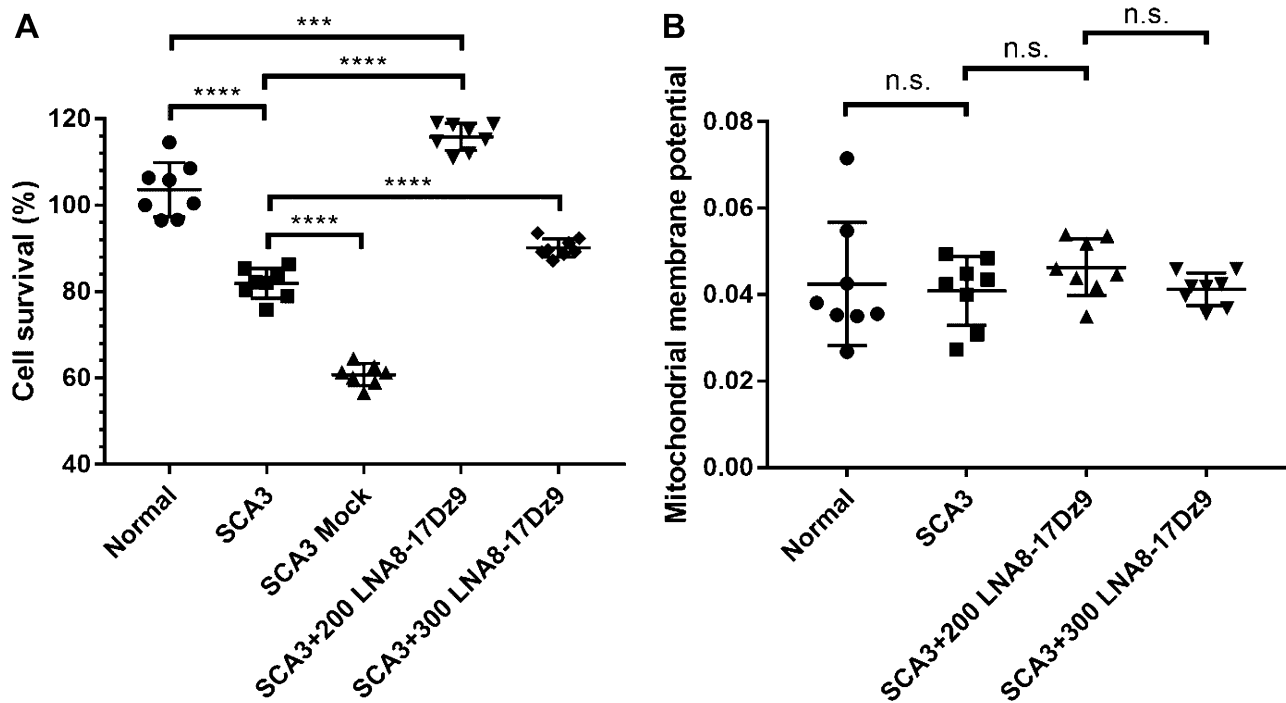


Fig. 6 DNAzyme treatment rescues SCA3 fibroblast cell survival and had no detrimental effects on mitochondrial polarization. **A** Cell proliferation assay of nucleofected SCA3 fibroblasts (200 or 300 pmol LNA8-17Dz9) in comparison to untreated normal fibroblasts, untreated

SCA3 cells, and mock-nucleofected SCA3 cells (2 biological replicates each with 4 technical replicates). **B** Mitochondrial depolarization assay using JC-10 dye (2 biological replicates each with 4 technical replicates)

cells. PINK1, PARKIN, and ATXN3 play important roles in mitochondrial maintenance and clearance [81, 82]. PINK1 is specifically activated by mitochondrial membrane potential depolarization, and recruits PARKIN to and activates PARKIN's ubiquitinase activity on damaged mitochondria [83]. ATXN3 deubiquitinates PARKIN directly and reduces the extent of PARKIN ubiquitination in cells [81]. To see if knockdown of wtATXN3 in SCA3 fibroblasts by DNAzyme could off-set PARKIN's ubiquitination on depolarized mitochondria and lead to accumulation of low-quality mitochondria, we measured mitochondrial membrane potential in DNAzyme-treated SCA3 fibroblasts and did not observe any change with respect to untreated or normal cells (Fig. 6B). As a result, we did not detect any oxidative DNA damage from mitochondrion-derived reactive oxygen species using 8-hydroxy-2-deoxyguanosine antibodies (8-OHdG, Fig. S14). Taken together, we demonstrate that allele-specific targeting of mutant polyQ protein can be achieved in SCA1 fibroblasts and the destruction of mutATXN3 outweighs the limited wtATXN3 reduction and significantly improves cell survival without compromising mitochondrial function in SCA3 fibroblasts.

We believe that enhanced delivery to target tissues/cells is an important area of research for translational application of DNAzyme. We explored two packaging/

delivery methods in this study, namely, the liposome DCL64 formulation and DNA tetrahedron. Despite the significantly increased cellular uptake in both blood–brain barrier endothelial and neuroblastoma cells (Fig. S15), the DCL64-packaged DNAzyme only reduced the mutant polyQ protein load by 20% (Fig. S15F). Given that the fluorescently tagged DNAzyme is retained within cells (Fig. S15A–D), it is possible that the payload is not sufficiently released from the endosome, possibly due to a lack of ionizable cations in the formulation [84]. Various DNA tetrahedral nanoparticles have successfully delivered payload into glioma, kidney, or alveolar epithelial cells [85–87]. However, the biological effect after delivery remains largely uninvestigated. We show that DNA tetrahedron-packaged DNAzyme did not significantly knock down target protein in neuron-like cells, suggesting that unfacilitated endocytosis of DNA nanoparticle is insufficient to achieve cellular efficacy at least in our tested model (Fig. S15F). With recent advances in lipid nanoparticle formulation and cell penetrating peptide conjugation, it is possible to broaden DNAzyme's biodistribution and bioavailability in animal models [88–91], even though a single or repeated injection of naked oligonucleotides already leads to a wide CNS spread in mice [30, 44].

Stereotaxically Injected LNA8-17Dz9 Knocks Down High Molecular Weight ATXN3 In vivo

To evaluate the stability of LNA8-17Dz9 in vivo, we administered a low dosage (25 μg) of Cy5-labeled DNAzyme in the right ventricle of 6-week old SCA3 MJD84.2 mice by stereotaxic injection. Among several well established SCA3 mouse models, the transgenic MJD84.2 mouse was chosen for the following studies because the YAC construct harbors a human *ATXN3* gene (with Q3KQ80 repeats) under its native promoter and the mouse exhibits disease-relevant neuropathological phenotype and behavioral abnormalities from 4 weeks of age [92, 93]. I.V.I.S. imaging was performed 48 h to 42 days post injection and suggests that the low-dose LNA8-17Dz9 is detectable in mouse brain for at least 1 month (Fig. 7A). However, we cannot rule out the possibility that the total fluorescence signal may overestimate the quantity of intact Cy5-labeled LNA8-17Dz9, as partially cleaved DNAzyme and free Cy5 may be present. Six-week old SCA3 mice

($n=4$) were subsequently injected with an intermediate dose (400 μg) of LNA8-17Dz9 in the same brain region. One month post injection, three of the four injected mice were harvested for immunoblotting and qRT-PCR and one for IF imaging (all from the right cortex). For comparison, age-matched WT mice and SCA3 mice injected with saline ($n=4$ for each) were used as controls. All the DNAzyme-injected mice survived and showed no signs of toxicity (Table S2) or apparent gliosis (Fig. S16). By immunoblotting, we demonstrate that the LNA8-17Dz9 significantly reduced the HMW atxn3 accumulation [30, 34] by approximately 50% (Fig. 7B). At the tested dosage, we did not observe changes in the level of soluble, monomeric mut atxn3 and wt atxn3 but a 20% reduction of wt atxn2 (Fig. 7B). The wt tbp level post DNAzyme treatment was not significantly different from that of WT mouse (Fig. 7B), consistent with our observations in patient-derived fibroblast cells (Figs. 4 and 5). At an RNA level, we observed a general trend of reduction in the tested polyQ RNA (Fig. S17).

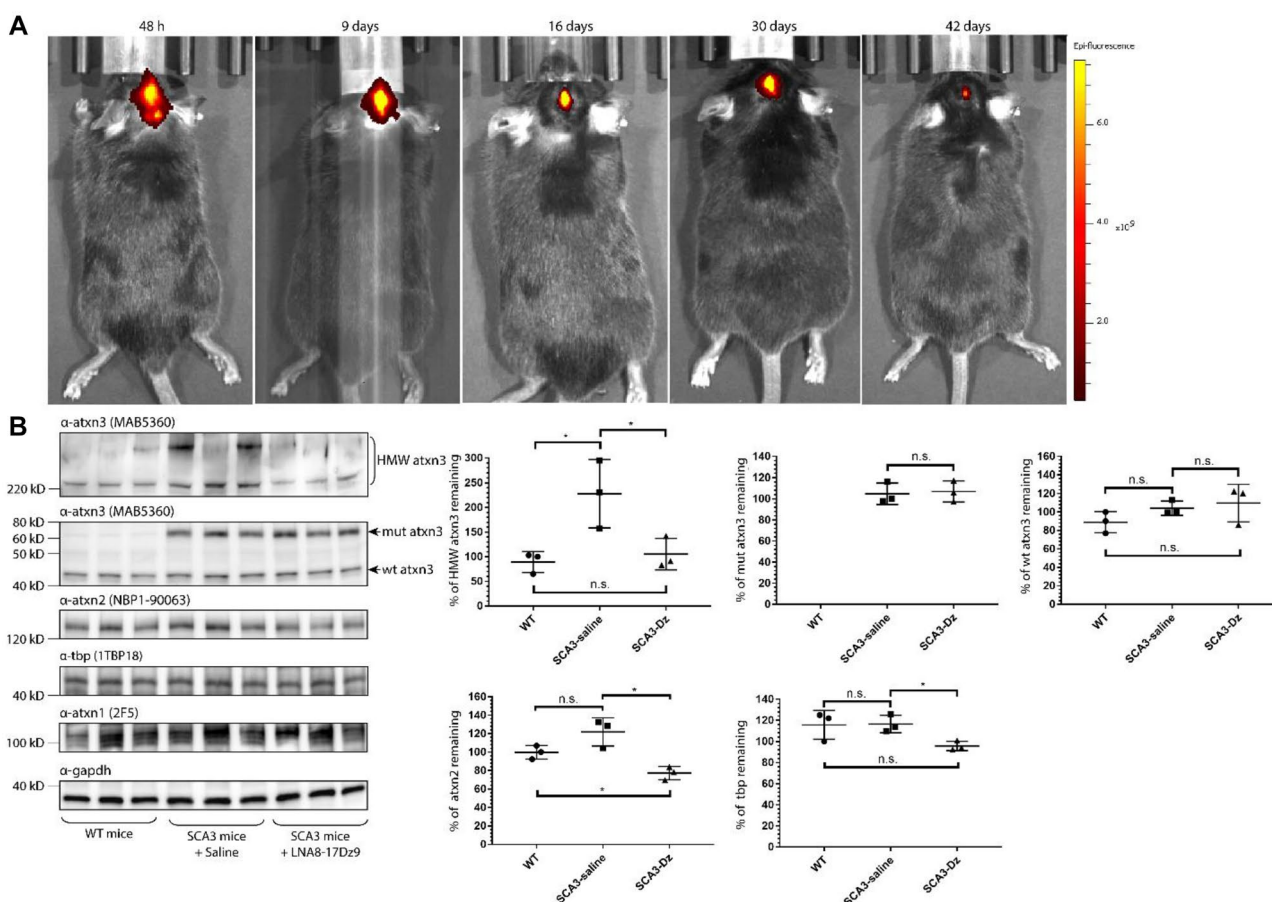


Fig. 7 DNAzyme reduces HMW ATXN3 in MJD84.2 mouse brain. **A** I.V.I.S. imaging of low-dosage (25 μg) Cy5-labeled LNA8-17Dz9 stereotaxically injected in a SCA3 right lateral ventricle. All images were normalized to the same fluorescent scale. **B** Immunoblot and

quantification of SCA3 mouse right cortex without treatment, with saline injection or with an intermediate dosage (400 μg) LNA8-17Dz9 ($n=3$). The protein level of ATXN1 was not quantified due to promiscuity of the antibody

Discussion

In this study, we have designed and optimized a repeat-based LNA-modified DNAzyme (LNA8-17Dz9) that can significantly reduce mutant polyQ RNA or protein load in several disease-related cell models and in one animal model. Our data provide the proof of principle that DNAzyme cleaves expanded CAG repeats of multiple polyQ diseases. The most significant difference between DNAzyme and other RNA silencing therapies is that it destroys target RNA without any auxiliary enzyme such as RNase H or the RNA-induced silencing complex (RISC). High-resolution computational modeling of human RNase H1 bound to an RNA/DNA hybrid indicates that the scissile phosphate aligns with the cleavage pocket and is approximately 9–10 nt from either end of the target RNA [94]. This distance coincides with the mismatched region (the 15-nt catalytic core and the T·G mismatch) of the LNA8-17Dz9 (Fig. 1A), likely distorting the local interaction network within the cleavage pocket and rendering RNase H ineffective. This may be analogous to RNA interference where imperfectly matched double-stranded RNA disrupts Argonaute 2 active site interaction and subsequently hinders cleavage [95, 96]. In contrast to elevated cell death through RNase H recruitment by a repeat-based LNA gapper [47], we observed improved cell proliferation after DNAzyme treatment (Fig. 6A). The ability of DNAzyme to cleave RNA without any protein component avoids overburdening cellular machinery.

Mutant protein knockdown by LNA8-17Dz9 is best achieved in neuronal cells (iNeuron and neuroblastoma, > 90%), followed by kidney embryonic cells (HEK293, 80–100%), patient-derived fibroblasts (SCA1 and SCA3, 40–60%), and patient-derived iPSCs (SCA3, 50%). We estimate the transfection efficiency of DNAzyme into each cell type is as follows: patient-derived fibroblasts (80–90%), kidney embryonic cells (80–90%), neuroblastoma cells (50–60%), patient-derived iPSCs (30–40%), and iNeurons (< 10%). A direct correlation between transfection efficiency and target knockdown in each cell type may be difficult, as in some cell types the target RNA/protein is endogenously expressed while in others ectopically expressed. In addition, the target RNA/protein expression level and/or accessibility to DNAzyme may vary significantly in different cell types. And it is difficult to assess how efficiently DNAzymes escape from the endosome in different cell types. However, the greatest knockdown in neuronal cells infers that LNA8-17Dz9 is suitable for therapeutic application to neurodegenerative disorders. Previous ASO studies suggest that complete inhibition of mutant protein is not necessary and partial non-allelic reduction of mutHTT by 20–40%, mutATXN1 by 20% and

mutATXN3 by 30% in mouse brain could already reverse molecular, phenotypic, and/or behavioral defects [30, 44, 97, 98]. We further demonstrate in a SCA3 mouse model that stereotaxically administered LNA8-17Dz9 (1) is stable for at least 1 month in mouse brain (tested at a low dosage), (2) neither shows toxic effects nor causes early death (tested at an intermediate dosage), and (3) reduces the HMW ATXN3 proteins by approximately 50% (tested at an intermediate dosage). We hypothesize that by increasing the administered dose of DNAzyme (> 750 µg per animal) more efficient target RNA/protein knockdown can be achieved by promoting the bioavailability in local tissue. Further examination of off-target effects, by performing RNAseq using mouse brains, molecular and behavioral rescue, and toxicity, by performing acute and long-term toxicological profiles, will be carried out using a larger sample size.

One of the main drawbacks of targeting CAG repeat RNA is the potential lack of specificity—short CAG repeats are present in the normal target allele as well as > 1000 genes [99]. By performing RNAseq on mock- and LNA8-17Dz9-nucleofected normal fibroblasts, we observed no significant alteration of > 60 published mRNA containing different CAG repeat lengths at a transcriptional level (Table S1). The rationale for allele-specific knockdown using LNA8-17Dz9 is that the expanded CAG RNA contains more binding sites and that its 3D folding is energetically different from that of short CAG repeats for targeting [48]. Indeed, we successfully demonstrate that LNA8-17Dz9 specifically knocks down 40–60% mutATXN1 in SCA1 fibroblasts without affecting the endogenous ATXN1 or ATXN3 protein levels (Fig. 4A). Allele-specific targeting of mutATXN1 by LNA8-17Dz9 is beneficial because mice lacking Ataxin1 display learning deficits [100]. However, we did observe a 20–40% knockdown of endogenous ATXN2 and TBP, which is consistently reproduced in both SCA1 and SCA3 fibroblasts (Figs. 4 and 5). The 20–40% ATXN2 knockdown should be well-tolerated because *Atxn2*-KO mice display normal weight, lifespan, exploratory patterns, and spatial learning, and *Atxn2*-knockdown TDP43 transgene mice exhibit increase lifespan by 35% [101, 102]. The 20–40% knockdown of TBP in SCA1/SCA3 fibroblasts brings the protein level similar to normal fibroblasts (Figs. 4 and 5), which is consistently reproduced in the SCA3 mouse model (Fig. 7B). In SCA3 fibroblasts and iPSCs, ATXN3 was knocked down by 40–60% non-allele-specifically by LNA8-17Dz9 (Figs. 3E and 4B). Given that Ataxin3 is not essential for mouse viability and fertility [75, 76], the observed reduction of ATXN3 should be well-tolerated. However, we do not anticipate detrimental consequences because (1) DNAzyme treatment improves SCA3 cell

survival without affecting mitochondrial function or p62-dependent autophagy (Figs. 5 and S11), (2) DNAzyme-treated fibroblasts show no significant RNAseq difference of > 60 CAG-containing mRNA when compared to mock-treated cells (Table S1), (3) knockdown of endogenous genes expressing short CAG repeats by an LNA ASO in WT mice did not generate toxicity or attenuate cell function [103], and (4) the DNAzyme-treated SCA3 mice did not show acute toxicity or death.

LNA8-17Dz9 is restricted to cleavage between adenine (A) and guanine (G). The 10–23 DNAzyme (10-23Dz) cleaves any purine–pyrimidine (RY, R = A or G; Y = U or C) junction and may be tried for a wide variety of diseases [104]. The RY cleavage efficiency is in the order of AU = GU ≥ GC >> AC [105]. The 10-23Dz may cleave the expanded CUG repeat in myotonic dystrophy 1 (DM1 [106]) and Fuchs endothelial corneal dystrophy (FECD [107]) at GC sites, the intronic CCUG repeat in myotonic dystrophy 2 (DM2 [108]) and GGGGCC repeat in C9orf72-amyotrophic lateral sclerosis/ frontotemporal dementia (ALS/FTD [109]) at GC sites, the CGG repeat in Fragile X-associated tremor ataxia syndrome (FXTAS [110]) and oculopharyngodistal myopathy (OPDM [111]) at GC sites, and the AU-rich repeats in SCA10 [112], SCA31 [113], and SCA37 [114] at AU sites. Combining 8-17DZ and 10-23Dz, DNAzymes can target most, if not all, expanded microsatellite repeats in gain-of-function disorders.

In conclusion, using a single therapeutic DNAzyme to treat potentially a panel of polyQ neurodegenerative diseases is attractive, as it greatly simplifies the processes of rational design, pharmacodynamic and kinetic validation, and manufacture. More focused chemical modifications can be tailored to the same agent without variations arising from sequence changes. Moreover, repeat-based targeting may offer unexpected advantages over strategies that target unique sequences (or single-nucleotide polymorphisms, SNPs). This is because the potency of targeting unique sequences is greatly influenced by RNA processing dynamics and isoform structure, and the potency is consistently reduced in SCA3 and SBMA mice derived from cDNA transgenes but not so in animals derived from full-length transgenes [34, 115, 116]. Although DNAzyme can be reprogrammed to recognize SNPs, extensive genotyping needs to be performed to identify SNPs sufficiently present in the majority of patients. For instance, it has been estimated that 5–7 allele-specific oligonucleotides are needed to cover 75–85.6% of HD patients [117–119]. Combining multiple DNAzymes into a single therapy with regulatory approval may be difficult. It could be challenging when no SNPs associated with polyQ mutation can be identified (such as SCA2) [120], when the SNP-targeting oligonucleotide does not show intended allelic selectivity [121], or when patients are

homozygous for the targeted SNPs. Hence, repeat-based DNAzyme provides new hope for currently incurable polyQ neurodegeneration and its reprogrammability can extend to other diseases with RNA pathology or etiology.

Abbreviations 8-OHdG: 8-Hydroxy-2-deoxyguanosine; ASO: Antisense oligonucleotide; ATXN1: Ataxin 1; ATXN2: Ataxin 2; ATXN3: Ataxin 3; ATXN7: Ataxin 7; CNS: Central nervous system; DPPC: 1,2-Dipalmitoyl-sn-glycero-3-phosphocoline; DRPLA: Dentatorubropallidoluysian atrophy; Dz: DNAzyme; eGFP: Enhanced green fluorescent protein; HD: Huntington's disease; HMW: High molecular weight; hNGN2: Human neurogenin 2; HTT: Huntingtin; HTTex1: HTT exon 1; i.c.v.: Intracerebroventricular; IF: Immunofluorescence; iNeuron: Induced neuron; iPSC: Induced pluripotent stem cell; I.V.I.S: In vivo imaging system; LNA: Locked nucleic acid; Mut: Mutant; PNA: Peptide nucleic acid; polyQ: Polyglutamine; P/S: Penicillin–streptomycin; RAN: Noncanonical repeat-associated non-ATG; SBMA: Spinobulbar muscular atrophy; SCA: Spinocerebellar ataxia; TBP: TATA binding protein; Wt: Wildtype

Supplementary Information The online version contains supplementary material available at <https://doi.org/10.1007/s13311-021-01075-w>.

Required Author Forms Disclosure forms provided by the authors are available with the online version of this article.

Author Contribution N.Z. and T.A. designed the experiments. N.Z. and J.S. performed the in vitro cleavage assays. J.S. and K.A. performed the ASO experiments. N.Z. and B.B. performed qRT-PCR and IF. B.B. performed the liposome packaging and total RNA extractions. N.Z. and J.S. performed the immunoblotting and cell proliferation studies. R.K. performed the iNeuron differentiation and transfection. G.B.X. generated the SCA3 iPSC line. N.Z., B.B., and A.T. performed the in vivo studies. N.Z. and A.J.Z. performed the RNAseq analysis. K.Y. provided the BMEC cell line and training on stereotaxic injections. N.Z. performed the DNA tetrahedral assembly. All the authors contributed to the writing of this manuscript.

Funding This work was supported by a National Ataxia Foundation Young Investigator-SCA Award (#93000) to N.Z., a Foster Research Fund to T.A., National Institute on Aging of the National Institutes of Health grant (R21AG064567) to R.K., and the National Institutes of Health grants (RO1 NS079541-01 and RO1 EY026089-01A1) to P.S.S.

Data Availability The datasets used and/or analyzed in the current study are available from the corresponding author on reasonable request.

Declarations

Ethics Approval and Consent to Participate All animal procedures were approved by the Houston Methodist Institutional Animal Care and Use Committee and conducted in compliance with the National Institutes of Health guidelines for the use of experimental animals. The study of SCA3 iPSC was approved by the University of Florida Institutional Review Board. The SCA3 subject was provided with the approved informed consent.

Consent for Publication All the authors read and approved the final manuscript.

Conflict of Interest The authors declare no competing interests.

Open Access This article is licensed under a Creative Commons Attribution 4.0 International License, which permits use, sharing, adaptation, distribution and reproduction in any medium or format, as long as you give appropriate credit to the original author(s) and the source, provide a link to the Creative Commons licence, and indicate if changes were made. The images or other third party material in this article are included in the article's Creative Commons licence, unless indicated otherwise in a credit line to the material. If material is not included in the article's Creative Commons licence and your intended use is not permitted by statutory regulation or exceeds the permitted use, you will need to obtain permission directly from the copyright holder. To view a copy of this licence, visit <http://creativecommons.org/licenses/by/4.0/>.

References

- Santoro SW, Joyce GF: **A general purpose RNA-cleaving DNA enzyme.** *Proc Natl Acad Sci U S A* 1997, **94**:4262-4266.
- Liu H, Yu X, Chen Y, Zhang J, Wu B, Zheng L, Haruehanroengra P, Wang R, Li S, Lin J, et al: **Crystal structure of an RNA-cleaving DNAzyme.** *Nat Commun* 2017, **8**:2006.
- Zhang N, Ashizawa T: **RNA toxicity and foci formation in microsatellite expansion diseases.** *Curr Opin Genet Dev* 2017, **44**:17-29.
- Chatterjee A, Saha S, Chakraborty A, Silva-Fernandes A, Mandal SM, Neves-Carvalho A, Liu Y, Pandita RK, Hegde ML, Hegde PM, et al: **The role of the mammalian DNA end-processing enzyme polynucleotide kinase 3'-phosphatase in spinocerebellar ataxia type 3 pathogenesis.** *PLoS Genet* 2015, **11**:e1004749.
- Enokido Y, Tamura T, Ito H, Arumughan A, Komuro A, Shiwaku H, Sone M, Foulle R, Sawada H, Ishiguro H, et al: **Mutant huntingtin impairs Ku70-mediated DNA repair.** *J Cell Biol* 2010, **189**:425-443.
- Fujita K, Nakamura Y, Oka T, Ito H, Tamura T, Tagawa K, Sasabe T, Katsuta A, Motoki K, Shiwaku H, et al: **A functional deficiency of TERA/VCP/p97 contributes to impaired DNA repair in multiple polyglutamine diseases.** *Nat Commun* 2013, **4**:1816.
- Gao R, Liu Y, Silva-Fernandes A, Fang X, Paulucci-Holthausen A, Chatterjee A, Zhang HL, Matsuura T, Choudhary S, Ashizawa T, et al: **Inactivation of PNKP by mutant ATXN3 triggers apoptosis by activating the DNA damage-response pathway in SCA3.** *PLoS Genet* 2015, **11**:e1004834.
- Illuzzi J, Yerkes S, Parekh-Olmedo H, Kmiec EB: **DNA breakage and induction of DNA damage response proteins precede the appearance of visible mutant huntingtin aggregates.** *J Neurosci Res* 2009, **87**:733-747.
- Qi ML, Tagawa K, Enokido Y, Yoshimura N, Wada Y, Watase K, Ishiura S, Kanazawa I, Botas J, Saitoe M, et al: **Proteome analysis of soluble nuclear proteins reveals that HMGB1/2 suppress genotoxic stress in polyglutamine diseases.** *Nat Cell Biol* 2007, **9**:402-414.
- Ashkenazi A, Bento CF, Ricketts T, Vicinanza M, Siddiqi F, Pavel M, Squitieri F, Hardenberg MC, Imarisio S, Menzies FM, Rubinsztein DC: **Polyglutamine tracts regulate beclin 1-dependent autophagy.** *Nature* 2017, **545**:108-111.
- Bence NF, Sampat RM, Kopito RR: **Impairment of the ubiquitin-proteasome system by protein aggregation.** *Science* 2001, **292**:1552-1555.
- Gidalevitz T, Ben-Zvi A, Ho KH, Brignull HR, Morimoto RI: **Progressive disruption of cellular protein folding in models of polyglutamine diseases.** *Science* 2006, **311**:1471-1474.
- Kuiper EF, de Mattos EP, Jardim LB, Kampinga HH, Bergink S: **Chaperones in Polyglutamine Aggregation: Beyond the Q-Stretch.** *Front Neurosci* 2017, **11**:145.
- Benn CL, Sun T, Sadri-Vakili G, McFarland KN, DiRocco DP, Yohrling GJ, Clark TW, Bouzou B, Cha JH: **Huntingtin modulates transcription, occupies gene promoters in vivo, and binds directly to DNA in a polyglutamine-dependent manner.** *J Neurosci* 2008, **28**:10720-10733.
- Chen-Plotkin AS, Sadri-Vakili G, Yohrling GJ, Braveman MW, Benn CL, Glajch KE, DiRocco DP, Farrell LA, Krainc D, Gines S, et al: **Decreased association of the transcription factor Sp1 with genes downregulated in Huntington's disease.** *Neurobiol Dis* 2006, **22**:233-241.
- Gasset-Rosa F, Chillon-Marinhas C, Goginashvili A, Atwal RS, Artates JW, Tabet R, Wheeler VC, Bang AG, Cleveland DW, Lagier-Tourenne C: **Polyglutamine-Expanded Huntingtin Exacerbates Age-Related Disruption of Nuclear Integrity and Nucleocytoplasmic Transport.** *Neuron* 2017, **94**:48-57 e44.
- Klement IA, Skinner PJ, Kaytor MD, Yi H, Hersch SM, Clark HB, Zoghbi HY, Orr HT: **Ataxin-1 nuclear localization and aggregation: role in polyglutamine-induced disease in SCA1 transgenic mice.** *Cell* 1998, **95**:41-53.
- Burke KA, Kauffman KJ, Umbaugh CS, Frey SL, Legleiter J: **The interaction of polyglutamine peptides with lipid membranes is regulated by flanking sequences associated with huntingtin.** *J Biol Chem* 2013, **288**:14993-15005.
- Gao X, Campbell WA, Chaibva M, Jain P, Leslie AE, Frey SL, Legleiter J: **Cholesterol Modifies Huntingtin Binding to, Disruption of, and Aggregation on Lipid Membranes.** *Biochemistry* 2016, **55**:92-102.
- Grima JC, Daigle JG, Arbez N, Cunningham KC, Zhang K, Ochaba J, Geater C, Morozko E, Stocksdales J, Glatzer JC, et al: **Mutant Huntingtin Disrupts the Nuclear Pore Complex.** *Neuron* 2017, **94**:93-107 e106.
- Costa V, Giacomello M, Hudec R, Lopreiato R, Ermak G, Lim D, Malorni W, Davies KJ, Carafoli E, Scorrano L: **Mitochondrial fission and cristae disruption increase the response of cell models of Huntington's disease to apoptotic stimuli.** *EMBO Mol Med* 2010, **2**:490-503.
- Orr AL, Li S, Wang CE, Li H, Wang J, Rong J, Xu X, Mastroberardino PG, Greenamyre JT, Li XJ: **N-terminal mutant huntingtin associates with mitochondria and impairs mitochondrial trafficking.** *J Neurosci* 2008, **28**:2783-2792.
- Panov AV, Gutekunst CA, Leavitt BR, Hayden MR, Burke JR, Strittmatter WJ, Greenamyre JT: **Early mitochondrial calcium defects in Huntington's disease are a direct effect of polyglutamines.** *Nat Neurosci* 2002, **5**:731-736.
- Banez-Coronel M, Ayhan F, Tarabochia AD, Zu T, Perez BA, Tusi SK, Pletnikova O, Borchelt DR, Ross CA, Margolis RL, et al: **RAN Translation in Huntington Disease.** *Neuron* 2015, **88**:667-677.
- Cleary JD, Pattamatta A, Ranum LPW: **Repeat-associated non-ATG (RAN) translation.** *J Biol Chem* 2018, **293**:16127-16141.
- Cleary JD, Ranum LP: **New developments in RAN translation: insights from multiple diseases.** *Curr Opin Genet Dev* 2017, **44**:125-134.
- Dabrowska M, Juzwa W, Krzyzosiak WJ, Olejniczak M: **Precise Excision of the CAG Tract from the Huntingtin Gene by Cas9 Nickases.** *Front Neurosci* 2018, **12**:75.
- Kolli N, Lu M, Maiti P, Rosignol J, Dunbar GL: **CRISPR-Cas9 Mediated Gene-Silencing of the Mutant Huntingtin Gene in an In Vitro Model of Huntington's Disease.** *Int J Mol Sci* 2017, **18**.
- Marthaler AG, Tubsuwan A, Schmid B, Poulsen UB, Engelbrecht AF, Mau-Holzmann UA, Hyttel P, Nielsen TT, Nielsen JE, Holst B: **Generation of an isogenic, gene-corrected control cell line**

- of the spinocerebellar ataxia type 2 patient-derived iPSC line H266.** *Stem Cell Res* 2016, **16**:202-205.
30. McLoughlin HS, Moore LR, Chopra R, Komlo R, McKenzie M, Blumenstein KG, Zhao H, Kordasiewicz HB, Shakkottai VG, Paulson HL: **Oligonucleotide therapy mitigates disease in spinocerebellar ataxia type 3 mice.** *Ann Neurol* 2018, **84**:64-77.
 31. Merienne N, Vachey G, de Longprez L, Meunier C, Zimmer V, Perriard G, Canales M, Mathias A, Herrgott L, Beltraminelli T, et al: **The Self-Inactivating KamiCas9 System for the Editing of CNS Disease Genes.** *Cell Rep* 2017, **20**:2980-2991.
 32. Monteys AM, Ebanks SA, Keiser MS, Davidson BL: **CRISPR/Cas9 Editing of the Mutant Huntingtin Allele In Vitro and In Vivo.** *Molecular Therapy* 2017, **25**:12-23.
 33. Moore LR, Keller L, Bushart DD, Delatorre RG, Li D, McLoughlin HS, do Carmo Costa M, Shakkottai VG, Smith GD, Paulson HL: **Antisense oligonucleotide therapy rescues aggregates formation in a novel spinocerebellar ataxia type 3 human embryonic stem cell line.** *Stem Cell Res* 2019, **39**:101504.
 34. Moore LR, Rajpal G, Dillingham IT, Qutob M, Blumenstein KG, Gattis D, Hung G, Kordasiewicz HB, Paulson HL, McLoughlin HS: **Evaluation of Antisense Oligonucleotides Targeting ATXN3 in SCA3 Mouse Models.** *Mol Ther Nucleic Acids* 2017, **7**:200-210.
 35. Ouyang S, Xie Y, Xiong Z, Yang Y, Xian Y, Ou Z, Song B, Chen Y, Xie Y, Li H, Sun X: **CRISPR/Cas9-Targeted Deletion of Polyglutamine in Spinocerebellar Ataxia Type 3-Derived Induced Pluripotent Stem Cells.** *Stem Cells Dev* 2018, **27**:756-770.
 36. Scoles DR, Meera P, Schneider MD, Paul S, Dansithong W, Figueroa KP, Hung G, Rigo F, Bennett CF, Otis TS, Pulst SM: **Antisense oligonucleotide therapy for spinocerebellar ataxia type 2.** *Nature* 2017, **544**:362-366.
 37. Tabrizi SJ, Smith AV, Bennett CF: **Targeting Huntingtin in Patients with Huntington's Disease. Reply.** *N Engl J Med* 2019, **381**:1181-1182.
 38. Yang S, Chang R, Yang H, Zhao T, Hong Y, Kong HE, Sun X, Qin Z, Jin P, Li S, Li XJ: **CRISPR/Cas9-mediated gene editing ameliorates neurotoxicity in mouse model of Huntington's disease.** *J Clin Invest* 2017, **127**:2719-2724.
 39. Anzalone AV, Randolph PB, Davis JR, Sousa AA, Koblan LW, Levy JM, Chen PJ, Wilson C, Newby GA, Raguram A, Liu DR: **Search-and-replace genome editing without double-strand breaks or donor DNA.** *Nature* 2019.
 40. Komor AC, Badran AH, Liu DR: **CRISPR-Based Technologies for the Manipulation of Eukaryotic Genomes.** *Cell* 2017, **169**:559.
 41. Liu C, Zhang L, Liu H, Cheng K: **Delivery strategies of the CRISPR-Cas9 gene-editing system for therapeutic applications.** *J Control Release* 2017, **266**:17-26.
 42. Bengtsson NE, Hall JK, Odom GL, Phelps MP, Andrus CR, Hawkins RD, Hauschka SD, Chamberlain JR, Chamberlain JS: **Muscle-specific CRISPR/Cas9 dystrophin gene editing ameliorates pathophysiology in a mouse model for Duchenne muscular dystrophy.** *Nat Commun* 2017, **8**:14454.
 43. Friedrich J, Kordasiewicz HB, O'Callaghan B, Handler HP, Wagener C, Duvick L, Swayze EE, Rainwater O, Hofstra B, Benneyworth M, et al: **Antisense oligonucleotide-mediated ataxin-1 reduction prolongs survival in SCA1 mice and reveals disease-associated transcriptome profiles.** *JCI Insight* 2018, **3**.
 44. Kordasiewicz HB, Stanek LM, Wancewicz EV, Mazur C, McAlonis MM, Pytel KA, Artates JW, Weiss A, Cheng SH, Shihabuddin LS, et al: **Sustained therapeutic reversal of Huntington's disease by transient repression of huntingtin synthesis.** *Neuron* 2012, **74**:1031-1044.
 45. Niu C, Prakash TP, Kim A, Quach JL, Huryn LA, Yang Y, Lopez E, Jazayeri A, Hung G, Sopher BL, et al: **Antisense oligonucleotides targeting mutant Ataxin-7 restore visual function in a mouse model of spinocerebellar ataxia type 7.** *Sci Transl Med* 2018, **10**.
 46. Datson NA, Gonzalez-Barriga A, Kourkouta E, Weij R, van de Giessen J, Mulders S, Kontkanen O, Heikkinen T, Lehtimäki K, van Deutekom JC: **The expanded CAG repeat in the huntingtin gene as target for therapeutic RNA modulation throughout the HD mouse brain.** *PLoS One* 2017, **12**:e0171127.
 47. Gagnon KT, Watts JK, Pendergraft HM, Montailier C, Thai D, Potier P, Corey DR: **Antisense and antigene inhibition of gene expression by cell-permeable oligonucleotide-oligospermine conjugates.** *J Am Chem Soc* 2011, **133**:8404-8407.
 48. Hu J, Matsui M, Gagnon KT, Schwartz JC, Gabillet S, Arar K, Wu J, Bezprozvanny I, Corey DR: **Allele-specific silencing of mutant huntingtin and ataxin-3 genes by targeting expanded CAG repeats in mRNAs.** *Nat Biotechnol* 2009, **27**:478-484.
 49. Fernandopulle MS, Prestil R, Grunseich C, Wang C, Gan L, Ward ME: **Transcription Factor-Mediated Differentiation of Human iPSCs into Neurons.** *Curr Protoc Cell Biol* 2018, **79**:e51.
 50. Xia G, Santostefano K, Hamazaki T, Liu J, Subramony SH, Terada N, Ashizawa T: **Generation of human-induced pluripotent stem cells to model spinocerebellar ataxia type 2 in vitro.** *J Mol Neurosci* 2013, **51**:237-248.
 51. Brown AK, Li J, Pavot CMB, Lu Y: **A lead-dependent DNAzyme with a two-step mechanism.** *Biochemistry* 2003, **42**:7152-7161.
 52. Romani AM: **Cellular magnesium homeostasis.** *Arch Biochem Biophys* 2011, **512**:1-23.
 53. Ryschon TW, Rosenstein DL, Rubinow DR, Niemela JE, Elin RJ, Balaban RS: **Relationship between skeletal muscle intracellular ionized magnesium and measurements of blood magnesium.** *J Lab Clin Med* 1996, **127**:207-213.
 54. Wolf FI, Trapani V: **Cell (patho)physiology of magnesium.** *Clin Sci (Lond)* 2008, **114**:27-35.
 55. Iotti S, Frassinetti C, Alderighi L, Sabatini A, Vacca A, Barbiroli B: **In vivo assessment of free magnesium concentration in human brain by 31P MRS. A new calibration curve based on a mathematical algorithm.** *NMR Biomed* 1996, **9**:24-32.
 56. Korolev N, Lyubartsev AP, Rupprecht A, Nordenskiöld L: **Competitive binding of Mg²⁺, Ca²⁺, Na⁺, and K⁺ ions to DNA in oriented DNA fibers: experimental and Monte Carlo simulation results.** *Biophys J* 1999, **77**:2736-2749.
 57. Bagur R, Hajnoczky G: **Intracellular Ca(2+) Sensing: Its Role in Calcium Homeostasis and Signaling.** *Mol Cell* 2017, **66**:780-788.
 58. Zhou W, Vazin M, Yu T, Ding J, Liu J: **In Vitro Selection of Chromium-Dependent DNAszymes for Sensing Chromium(III) and Chromium(VI).** *Chemistry* 2016, **22**:9835-9840.
 59. Adams BD, Parsons C, Walker L, Zhang WC, Slack FJ: **Targeting noncoding RNAs in disease.** *J Clin Invest* 2017, **127**:761-771.
 60. Hegarty JP, Stewart DB, Sr.: **Advances in therapeutic bacterial antisense biotechnology.** *Appl Microbiol Biotechnol* 2018, **102**:1055-1065.
 61. Sardone V, Zhou H, Muntoni F, Ferlini A, Falzarano MS: **Antisense Oligonucleotide-Based Therapy for Neuromuscular Disease.** *Molecules* 2017, **22**.
 62. Wurster CD, Ludolph AC: **Antisense oligonucleotides in neurological disorders.** *Ther Adv Neurol Disord* 2018, **11**:1756286418776932.
 63. Kim HK, Liu J, Li J, Nagraj N, Li M, Pavot CM, Lu Y: **Metal-dependent global folding and activity of the 8-17 DNAszyme studied by fluorescence resonance energy transfer.** *J Am Chem Soc* 2007, **129**:6896-6902.

64. Finkbeiner S: **Huntington's Disease**. *Cold Spring Harb Perspect Biol* 2011, **3**.
65. Landles C, Sathasivam K, Weiss A, Woodman B, Moffitt H, Finkbeiner S, Sun B, Gafni J, Ellerby LM, Trotter Y, et al: **Proteolysis of mutant huntingtin produces an exon 1 fragment that accumulates as an aggregated protein in neuronal nuclei in Huntington disease**. *J Biol Chem* 2010, **285**:8808-8823.
66. Estrada-Sanchez AM, Rebec GV: **Role of cerebral cortex in the neuropathology of Huntington's disease**. *Front Neural Circuits* 2013, **7**:19.
67. Krencik R, Seo K, van Asperen JV, Basu N, Cvetkovic C, Barlas S, Chen R, Ludwig C, Wang C, Ward ME, et al: **Systematic Three-Dimensional Coculture Rapidly Recapitulates Interactions between Human Neurons and Astrocytes**. *Stem Cell Reports* 2017, **9**:1745-1753.
68. Cvetkovic C, Basu N, Krencik R: **Synaptic Microcircuit Modeling with 3D Cocultures of Astrocytes and Neurons from Human Pluripotent Stem Cells**. *J Vis Exp* 2018.
69. Costa MD, Paulson HL: **Toward understanding Machado-Joseph disease**. *Prog Neurobiol* 2012, **97**:239-257.
70. Burnett BG, Pittman RN: **The polyglutamine neurodegenerative protein ataxin 3 regulates aggresome formation**. *Proc Natl Acad Sci U S A* 2005, **102**:4330-4335.
71. Feng Q, Miao Y, Ge J, Yuan Y, Zuo Y, Qian L, Liu J, Cheng Q, Guo T, Zhang L, et al: **ATXN3 Positively Regulates Type I IFN Antiviral Response by Deubiquitinating and Stabilizing HDAC3**. *J Immunol* 2018, **201**:675-687.
72. Gao R, Chakraborty A, Geater C, Pradhan S, Gordon KL, Snowden J, Yuan S, Dickey AS, Choudhary S, Ashizawa T, et al: **Mutant huntingtin impairs PNKP and ATXN3, disrupting DNA repair and transcription**. *Elife* 2019, **8**.
73. Herzog LK, Kevei E, Marchante R, Bottcher C, Bindsboll C, Lystad AH, Pfeiffer A, Gierisch ME, Salomons FA, Simonsen A, et al: **The Machado-Joseph disease deubiquitylase ataxin-3 interacts with LC3C/GABARAP and promotes autophagy**. *Aging Cell* 2020, **19**:e13051.
74. Zhou L, Wang H, Chen D, Gao F, Ying Z, Wang G: **p62/sequestosome 1 regulates aggresome formation of pathogenic ataxin-3 with expanded polyglutamine**. *Int J Mol Sci* 2014, **15**:14997-15010.
75. Schmitt I, Linden M, Khazneh H, Evert BO, Breuer P, Klockgether T, Wuellner U: **Inactivation of the mouse Atxn3 (ataxin-3) gene increases protein ubiquitination**. *Biochem Biophys Res Commun* 2007, **362**:734-739.
76. Switonski PM, Fiszler A, Kazmierska K, Kurpisz M, Krzyzosiak WJ, Figiel M: **Mouse ataxin-3 functional knock-out model**. *Neuromolecular Med* 2011, **13**:54-65.
77. Mori F, Tanji K, Odagiri S, Toyoshima Y, Yoshida M, Kakita A, Takahashi H, Wakabayashi K: **Autophagy-related proteins (p62, NBR1 and LC3) in intranuclear inclusions in neurodegenerative diseases**. *Neurosci Lett* 2012, **522**:134-138.
78. Seidel K, den Dunnen WF, Schultz C, Paulson H, Frank S, de Vos RA, Brunt ER, Deller T, Kampinga HH, Rub U: **Axonal inclusions in spinocerebellar ataxia type 3**. *Acta Neuropathol* 2010, **120**:449-460.
79. Zeng L, Wang B, Merillat SA, Minakawa EN, Perkins MD, Ramani B, Tallaksen-Greene SJ, Costa MDC, Albin RL, Paulson HL: **Differential recruitment of UBQLN2 to nuclear inclusions in the polyglutamine diseases HD and SCA3**. *Neurobiol Dis* 2015, **82**:281-288.
80. Butland SL, Devon RS, Huang Y, Mead CL, Meynert AM, Neal SJ, Lee SS, Wilkinson A, Yang GS, Yuen MM, et al: **CAG-encoded polyglutamine length polymorphism in the human genome**. *BMC Genomics* 2007, **8**:126.
81. Durcan TM, Kontogiannina M, Thorarinsdottir T, Fallon L, Williams AJ, Djarmati A, Fantaneanu T, Paulson HL, Fon EA: **The Machado-Joseph disease-associated mutant form of ataxin-3 regulates parkin ubiquitination and stability**. *Hum Mol Genet* 2011, **20**:141-154.
82. Geisler S, Holmstrom KM, Skujat D, Fiesel FC, Rothfuss OC, Kahle PJ, Springer W: **PINK1/Parkin-mediated mitophagy is dependent on VDAC1 and p62/SQSTM1**. *Nature Cell Biology* 2010, **12**:119-U170.
83. Sauve V, Sung G, Soya N, Kozlov G, Blaimschein N, Miotto LS, Trempe JF, Lukacs GL, Gehring K: **Mechanism of parkin activation by phosphorylation (vol 25, pg 623, 2018)**. *Nature Structural & Molecular Biology* 2018, **25**:744-744.
84. Wittrup A, Ai A, Liu X, Hamar P, Trifonova R, Charisse K, Manoharan M, Kirchhausen T, Lieberman J: **Visualizing lipid-formulated siRNA release from endosomes and target gene knockdown**. *Nat Biotechnol* 2015, **33**:870-876.
85. Tian T, Li J, Xie C, Sun Y, Lei H, Liu X, Xia J, Shi J, Wang L, Lu W, Fan C: **Targeted Imaging of Brain Tumors with a Framework Nucleic Acid Probe**. *ACS Appl Mater Interfaces* 2018, **10**:3414-3420.
86. Walsh AS, Yin H, Erben CM, Wood MJ, Turberfield AJ: **DNA cage delivery to mammalian cells**. *ACS Nano* 2011, **5**:5427-5432.
87. Yang J, Jiang Q, He L, Zhan P, Liu Q, Liu S, Fu M, Liu J, Li C, Ding B: **Self-Assembled Double-Bundle DNA Tetrahedron for Efficient Antisense Delivery**. *ACS Appl Mater Interfaces* 2018, **10**:23693-23699.
88. Cheng Q, Wei T, Farbiak L, Johnson LT, Dilliard SA, Siegwart DJ: **Selective organ targeting (SORT) nanoparticles for tissue-specific mRNA delivery and CRISPR-Cas gene editing**. *Nat Nanotechnol* 2020, **15**:313-320.
89. Gait MJ, Arzumanov AA, McClorey G, Godfrey C, Betts C, Hammond S, Wood MJA: **Cell-Penetrating Peptide Conjugates of Steric Blocking Oligonucleotides as Therapeutics for Neuro-muscular Diseases from a Historical Perspective to Current Prospects of Treatment**. *Nucleic Acid Ther* 2019, **29**:1-12.
90. Hammond SM, Hazell G, Shabanpoor F, Saleh AF, Bowerman M, Sleigh JN, Meijboom KE, Zhou H, Muntoni F, Talbot K, et al: **Systemic peptide-mediated oligonucleotide therapy improves long-term survival in spinal muscular atrophy**. *Proc Natl Acad Sci U S A* 2016, **113**:10962-10967.
91. Patel S, Ashwanikumar N, Robinson E, Xia Y, Mihai C, Griffith JP, 3rd, Hou S, Esposito AA, Ketova T, Welscher K, et al: **Naturally-occurring cholesterol analogues in lipid nanoparticles induce polymorphic shape and enhance intracellular delivery of mRNA**. *Nat Commun* 2020, **11**:983.
92. Cemal CK, Carroll CJ, Lawrence L, Lowrie MB, Ruddle P, Al-Mahdawi S, King RH, Pook MA, Huxley C, Chamberlain S: **YAC transgenic mice carrying pathological alleles of the MJD1 locus exhibit a mild and slowly progressive cerebellar deficit**. *Hum Mol Genet* 2002, **11**:1075-1094.
93. Gould VFC: **Mouse Models of Spinocerebellar Ataxia Type 3 (Machado-Joseph Disease)**. *Neurotherapeutics* 2012, **9**:285-296.
94. Hyjek M, Figiel M, Nowotny M: **RNases H: Structure and mechanism**. *DNA Repair (Amst)* 2019, **84**:102672.
95. Du Q, Thonberg H, Wang J, Wahlestedt C, Liang Z: **A systematic analysis of the silencing effects of an active siRNA at all single-nucleotide mismatched target sites**. *Nucleic Acids Res* 2005, **33**:1671-1677.
96. Wang Y, Juranek S, Li H, Sheng G, Tuschl T, Patel DJ: **Structure of an argonaute silencing complex with a seed-containing guide DNA and target RNA duplex**. *Nature* 2008, **456**:921-926.
97. Jafar-Nejad P, Ward CS, Richman R, Orr HT, Zoghbi HY: **Regional rescue of spinocerebellar ataxia type 1 phenotypes by 14-3-3epsilon haploinsufficiency in mice underscores complex pathogenicity in neurodegeneration**. *Proc Natl Acad Sci U S A* 2011, **108**:2142-2147.

98. Park J, Al-Ramahi I, Tan Q, Mollema N, Diaz-Garcia JR, Gallego-Flores T, Lu HC, Lagalwar S, Duvick L, Kang H, et al: **RAS-MAPK-MSK1 pathway modulates ataxin 1 protein levels and toxicity in SCA1.** *Nature* 2013, **498**:325-331.
99. Kozłowski P, de Mezer M, Krzyzosiak WJ: **Trinucleotide repeats in human genome and exome.** *Nucleic Acids Res* 2010, **38**:4027-4039.
100. Matilla A, Roberson ED, Banfi S, Morales J, Armstrong DL, Burright EN, Orr HT, Sweatt JD, Zoghbi HY, Matzuk MM: **Mice lacking ataxin-1 display learning deficits and decreased hippocampal paired-pulse facilitation.** *J Neurosci* 1998, **18**:5508-5516.
101. Becker LA, Huang B, Bieri G, Ma R, Knowles DA, Jafar-Nejad P, Messing J, Kim HJ, Soriano A, Auburger G, et al: **Therapeutic reduction of ataxin-2 extends lifespan and reduces pathology in TDP-43 mice.** *Nature* 2017, **544**:367-371.
102. Huynh DP, Maalouf M, Silva AJ, Schweizer FE, Pulst SM: **Dissociated fear and spatial learning in mice with deficiency of ataxin-2.** *PLoS One* 2009, **4**:e6235.
103. Rue L, Banez-Coronel M, Creus-Muncunill J, Giralt A, Alcalá-Vida R, Mentxaka G, Kagerbauer B, Zomeno-Abellan MT, Aranda Z, Venturi V, et al: **Targeting CAG repeat RNAs reduces Huntington's disease phenotype independently of huntingtin levels.** *J Clin Invest* 2016, **126**:4319-4330.
104. Krug N, Hohlfeld JM, Kirsten AM, Kornmann O, Beeh KM, Kappeler D, Korn S, Ignatenko S, Timmer W, Rogon C, et al: **Allergen-induced asthmatic responses modified by a GATA3-specific DNase.** *N Engl J Med* 2015, **372**:1987-1995.
105. Cairns MJ, King A, Sun LQ: **Optimisation of the 10-23 DNase-substrate pairing interactions enhanced RNA cleavage activity at purine-cytosine target sites.** *Nucleic Acids Res* 2003, **31**:2883-2889.
106. Kurkiewicz A, Cooper A, McIlwaine E, Cumming SA, Adam B, Krahe R, Puymirat J, Schoser B, Timchenko L, Ashizawa T, et al: **Towards development of a statistical framework to evaluate myotonic dystrophy type 1 mRNA biomarkers in the context of a clinical trial.** *PLoS One* 2020, **15**:e0231000.
107. Hu J, Rong Z, Gong X, Zhou Z, Sharma VK, Xing C, Watts JK, Corey DR, Mootha VV: **Oligonucleotides targeting TCF4 triplet repeat expansion inhibit RNA foci and mis-splicing in Fuchs' dystrophy.** *Hum Mol Genet* 2018, **27**:1015-1026.
108. Benhamou RI, Angelbello AJ, Wang ET, Disney MD: **A Toxic RNA Catalyzes the Cellular Synthesis of Its Own Inhibitor, Shunting It to Endogenous Decay Pathways.** *Cell Chem Biol* 2020, **27**:223-231 e224.
109. Jiang J, Zhu Q, Gendron TF, Saberi S, McAlonis-Downes M, Seelman A, Stauffer JE, Jafar-Nejad P, Drenner K, Schulte D, et al: **Gain of Toxicity from ALS/FTD-Linked Repeat Expansions in C9ORF72 Is Alleviated by Antisense Oligonucleotides Targeting GGGGCC-Containing RNAs.** *Neuron* 2016, **90**:535-550.
110. Drozd M, Delhaye S, Maurin T, Castagnola S, Grossi M, Brau F, Jarjat M, Willemsen R, Capovilla M, Hukema RK, et al: **Reduction of Fmr1 mRNA Levels Rescues Pathological Features in Cortical Neurons in a Model of FXTAS.** *Mol Ther Nucleic Acids* 2019, **18**:546-553.
111. Ishiura H, Shibata S, Yoshimura J, Suzuki Y, Qu W, Doi K, Almansour MA, Kikuchi JK, Taira M, Mitsui J, et al: **Noncoding CGG repeat expansions in neuronal intranuclear inclusion disease, oculopharyngodistal myopathy and an overlapping disease.** *Nat Genet* 2019, **51**:1222-1232.
112. White MC, Gao R, Xu W, Mandal SM, Lim JG, Hazra TK, Wakamiya M, Edwards SF, Raskin S, Teive HA, et al: **Inactivation of hnRNP K by expanded intronic AUUCU repeat induces apoptosis via translocation of PKCdelta to mitochondria in spinocerebellar ataxia 10.** *PLoS Genet* 2010, **6**:e1000984.
113. Ishiguro T, Sato N, Ueyama M, Fujikake N, Sellier C, Kanegami A, Tokuda E, Zamiri B, Gall-Duncan T, Mirceta M, et al: **Regulatory Role of RNA Chaperone TDP-43 for RNA Misfolding and Repeat-Associated Translation in SCA31.** *Neuron* 2017, **94**:108-124 e107.
114. Seixas AI, Loureiro JR, Costa C, Ordóñez-Ugalde A, Marcelino H, Oliveira CL, Loureiro JL, Dhingra A, Brandao E, Cruz VT, et al: **A Pentanucleotide ATTTTC Repeat Insertion in the Non-coding Region of DAB1, Mapping to SCA37, Causes Spinocerebellar Ataxia.** *Am J Hum Genet* 2017, **101**:87-103.
115. Lieberman AP, Yu Z, Murray S, Peralta R, Low A, Guo S, Yu XX, Cortes CJ, Bennett CF, Monia BP, et al: **Peripheral androgen receptor gene suppression rescues disease in mouse models of spinal and bulbar muscular atrophy.** *Cell Rep* 2014, **7**:774-784.
116. Sahashi K, Katsuno M, Hung G, Adachi H, Kondo N, Nakatsuji H, Tohrai G, Iida M, Bennett CF, Sobue G: **Silencing neuronal mutant androgen receptor in a mouse model of spinal and bulbar muscular atrophy.** *Hum Mol Genet* 2015, **24**:5985-5994.
117. Kaemmerer WF, Grondin RC: **The effects of huntingtin-lowering: what do we know so far?** *Degener Neurol Neuro* 2019, **9**:3-17.
118. Lombardi MS, Jaspers L, Spronkmans C, Gellera C, Taroni F, Di Maria E, Donato SD, Kaemmerer WF: **A majority of Huntington's disease patients may be treatable by individualized allele-specific RNA interference.** *Exp Neurol* 2009, **217**:312-319.
119. Pfister EL, Kennington L, Straubhaar J, Wagh S, Liu W, DiFiglia M, Landwehrmeyer B, Vonsattel JP, Zamore PD, Aronin N: **Five siRNAs targeting three SNPs may provide therapy for three-quarters of Huntington's disease patients.** *Curr Biol* 2009, **19**:774-778.
120. Pulst SM: **Degenerative ataxias, from genes to therapies: The 2015 Cotzias Lecture.** *Neurology* 2016, **86**:2284-2290.
121. Toonen LJA, Rigo F, van Attikum H, van Roon-Mom WMC: **Antisense Oligonucleotide-Mediated Removal of the Polyglutamine Repeat in Spinocerebellar Ataxia Type 3 Mice.** *Mol Ther Nucleic Acids* 2017, **8**:232-242.

Publisher's Note Springer Nature remains neutral with regard to jurisdictional claims in published maps and institutional affiliations.